

Review

An Overview of Polymer-Supported Catalysts for Wastewater Treatment through Light-Driven Processes

Maria João Silva ¹, João Gomes ¹, Paula Ferreira ^{1,2} and Rui C. Martins ^{1,*}

¹ CIEPQPF—Chemical Engineering Processes and Forest Products Research Center, Department of Chemical Engineering, Faculty of Sciences and Technology, University of Coimbra, Rua Sílvio Lima, 3030-790 Coimbra, Portugal; mariaj@eq.uc.pt (M.J.S.); jgomes@eq.uc.pt (J.G.); paula.ferreira@isec.pt (P.F.)

² Department of Chemical and Biological Engineering, Coimbra Institute of Engineering (ISEC), Rua Pedro Nunes, 3030-199 Coimbra, Portugal

* Correspondence: martins@eq.uc.pt

Abstract: In recent years, alarm has been raised due to the presence of chemical contaminants of emerging concern (CECs) in water. This concern is due to the risks associated with their exposure, even in small amounts. These complex compounds cannot be removed or degraded by existing technologies in wastewater treatment plants. Therefore, advanced oxidation processes have been studied, with the objective of developing a technology capable of complementing the conventional water treatment plants. Heterogenous photocatalysis stands out for being a cost-effective and environmentally friendly process. However, its most common form (with suspended catalytic particles) requires time-consuming and costly downstream processes. Therefore, the heterogeneous photocatalysis process with a supported catalyst is preferable. Among the available supports, polymeric ones stand out due to their favorable characteristics, such as their transparency, flexibility and stability. This is a relatively novel process; therefore, there are still some gaps in the scientific knowledge. Thus, this review article aims to gather the existing information about this process and verify which questions are still to be answered.

Keywords: heterogenous photocatalysis; polymeric supports; CEC; wastewater treatment



Citation: Silva, M.J.; Gomes, J.; Ferreira, P.; Martins, R.C. An Overview of Polymer-Supported Catalysts for Wastewater Treatment through Light-Driven Processes. *Water* **2022**, *14*, 825. <https://doi.org/10.3390/w14050825>

Academic Editor: Alexandre T. Paulino

Received: 9 February 2022

Accepted: 4 March 2022

Published: 6 March 2022

Publisher's Note: MDPI stays neutral with regard to jurisdictional claims in published maps and institutional affiliations.



Copyright: © 2022 by the authors. Licensee MDPI, Basel, Switzerland. This article is an open access article distributed under the terms and conditions of the Creative Commons Attribution (CC BY) license (<https://creativecommons.org/licenses/by/4.0/>).

1. Introduction

Recently, wastewater treatment plants (WWTPs) have faced a new challenge—the presence of contaminants of emerging concern (CECs) in waters. ‘CEC’ is a standard term used to identify environmental risks related to the discharge of new pollutants (synthetic or naturally occurring chemicals or microorganisms), with unpredictable consequences, including a risk of severe damage, even at low concentrations [1–3]. Exposure to some kinds of CECs can cause complications in the reproductive and in the immune system, both in humans and aquatic life [2,4]. The presence of CECs in water can also trigger the occurrence of antibiotic resistance genes in bacteria [4]. Therefore, the removal of CECs from water is imperative. However, the existing conventional WWTPs technologies are not effective in eliminating CECs [1,5]; hence, the elimination of CECs requires advanced treatments.

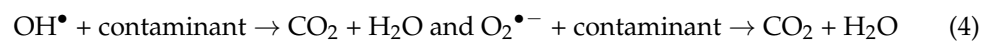
Advanced oxidation processes (AOPs) are highly effective in the oxidation of several organic and inorganic compounds. These processes are based on the generation of free radicals that successfully attack the pollutants, with elevated reaction rate constants [4,5]. Among the AOPs, photocatalysis stands out due to its advantages over other AOPs. Particularly, the Fenton process generates high amounts of sludge and is efficient at a narrow pH range (~3), which makes it difficult to operate with the inherent effluent pH [6,7]. As for ozone-based processes, they are considered expensive, not only due to the need to generate and burn O₃, but also because, to achieve high efficiencies, they need the addition of other reagents, such as H₂O₂, and radiation or catalysts [6,8].

Heterogeneous supported photocatalysis has become a promising technology to overcome the drawbacks of suspended photocatalysis. Suspended photocatalysts show advantages, such as a higher surface area and a higher reaction kinetic, which lead to higher photocatalytic efficiency over CEC abatement [9]. However, the separation and recovery of the photocatalyst may require expensive and time-consuming processes [9–11]. Heterogeneous photocatalysis with the immobilization of the catalyst on different substrates eliminates the need for these processes and minimizes the catalyst loss [10,11]. Additionally, the support can offer a high dispersion of the nanoparticle catalyst and simplify electron transfer, both of which contribute to better catalytic activities [11]. Among the various supports, polymeric materials are promising because of several advantages, such as a flexible nature, low cost, chemical resistance, mechanical stability, low density, high durability, and availability [10,12].

2. Polymer-Supported Photocatalysis Fundamentals

2.1. Reaction Mechanism

To understand any chemical process, it is essential to understand the reactions behind it. A simple, commonly proposed mechanism for the mineralization of the majority of organic contaminants by photocatalysis is illustrated with Equations (1)–(4). Firstly, generation of the photoinduced hole–electron pair ($h^+ - e^-$) in the catalyst surface occurs. Afterwards, water will react with the hole to form hydroxyl radicals (OH^\bullet), and oxygen reacts with the electron to form superoxide anion radicals ($O_2^{\bullet-}$); subsequently, these radicals interact with the contaminants [10,12].



2.2. Photocatalysts

Photocatalysis can be achieved using varied materials, commonly semiconductor oxides, because of their favorable light absorption abilities, electronic structures, charge transport features, and excited-state lifetimes [12]. Examples of these oxide materials include titanium dioxide (TiO_2), zinc oxide (ZnO), iron (III) oxide (Fe_2O_3), tungsten oxide (WO_3), and strontium titanate ($SrTiO_3$) [13].

2.2.1. Titanium Dioxide

TiO_2 is one of the most efficient photocatalysts, due to its properties of high stability, low cost, non-toxicity, and stability against photocorrosion [10,14]. In addition, it can be supported on various substrates [10,14]. However, due to its large band-gap (BG), TiO_2 is not able to absorb visible light [14,15]. Another drawback of TiO_2 -mediated photocatalysts is their rapid electron–hole recombination [12,15]. Nevertheless, the commercially available form of TiO_2 (P25) promotes efficient charge separation, due to its polymorphic characteristics. In addition, P25 is identified as the best TiO_2 catalyst, due to its crystallinity (80% anatase and 20% rutile) and its efficiency in OH^\bullet generation [16,17].

2.2.2. Zinc Oxide

ZnO is also a widely investigated semiconductor due to its abundance, low cost, and low toxicity [15]. The greatest advantage of ZnO as compared with TiO_2 is its ability to absorb a larger fraction of the UV spectrum, because its band gap is larger (3.3 eV) [15,18]. However, this disables the applications of visible light [14]. ZnO is also unstable in water, due to its intrinsic photocorrosion that leads to a weakening of $Zn^{2+} - O_2^-$ bonds and

produces O_2 and soluble Zn^{2+} [12,16]. Zn^{2+} rapidly dissolves in water to form $Zn(OH)_2$ on the ZnO surface, thus reducing the catalytic properties [12].

2.2.3. Iron (III) Oxide

Iron (III) oxide is currently considered a favorable semiconductor for photocatalytic reactions due to its low BG (2.3 eV) [19]. Therefore, unlike other photocatalysts such as ZnO and TiO_2 , it can use solar energy for photocatalytic applications [19,20]. In addition, Fe_2O_3 presents other advantages, such as excellent stability, recyclability, and abundance in the earth [19]. However, the usage of Fe_2O_3 has been restricted due to its low diffusion length, its high h^+e^- recombination rate, its hydrophobicity, and high surface energy that causes agglomeration and clump formation, increasing the particle size [20,21].

2.2.4. Tungsten Oxide

Tungsten trioxide has several allotropic forms, mainly two monoclinic structures, a triclinic structure and a hexagonal form [22]. These materials have their advantages and disadvantages: for example, triclinic WO_3 is only stable at low temperatures ($T < 17^\circ C$) [22,23], the accessibility to the internal surface is better for hexagonal WO_3 than for monoclinic WO_3 [22,24] and monoclinic WO_3 is more active than hexagonal WO_3 [22,24].

Compared with TiO_2 , which responds only to ultraviolet (UV) light, WO_3 is visible-light-responsive, due to the size of its BG (2.6–2.8 eV) [22,25]. However, tungsten oxide is only efficient for acid-catalyzed reactions due to its solid acidic and redox properties [25], and bare WO_3 is not very active due to the rapid recombination of photogenerated electrons and holes [22]. Fortunately, its efficiency is enhanced when a phase junction between hexagonal WO_3 and monoclinic WO_3 is formed [22,26].

2.2.5. Strontium Titanate

$SrTiO_3$ has a typical perovskite structure with advantages of a low cost and excellent chemical stability [27]. It has been widely used as a photocatalyst for water splitting and mineralization; however, due to the wide BG, it can only utilize UV light during photocatalytic reactions [27,28] and it presents a rapid recombination of photogenerated carriers [28].

Compared with TiO_2 , it has superior physical and chemical properties, such as chemical and structural stability, great heat resistance, corrosion resistance and easy modification by other substances [29].

2.3. Immobilization Techniques

Typically, heterogeneous photocatalysis uses powder nanoparticles of catalysts (the most common is TiO_2). This brings important difficulties when applying this technology in continuous or full-scale mode. There is a need to separate the powder material from the treated liquid, which entails some difficulties due to the low size of the catalyst particles [9–11]. Moreover, this will make catalyst recovery and reuse difficult [9–11]. Thus, to efficiently use a heterogeneous photocatalysis, the catalyst should be immobilized in a support. Among the potential supports, polymeric materials have interesting features due to their flexibility, transparency, and availability [10,12].

The photocatalyst can be immobilized either on the surface or in the polymer matrix, and it is important to know how the photocatalyst interacts with the polymer, in order to choose a suitable immobilization technique [9].

2.3.1. Immobilization on the Surface

Regarding the immobilization on the surface, the most applied method is dip-coating, which is based on the attachment of a thin layer of photocatalyst on the polymer surface [9], by immersion and withdrawing in a liquid solution, as shown in Figure 1a [9,30,31]. Subsequent evaporation of the solvent leaves behind a final dry coating on the substrate [30]. Even though this process minimizes the agglomeration, inexpensive, and simple, it also

has some disadvantages, such as a wide particle size distribution [9,30,31]. However, depending on the characteristics of the catalyst and the support, it may be necessary to modify the surface of the support to allow better adhesion to the catalyst.

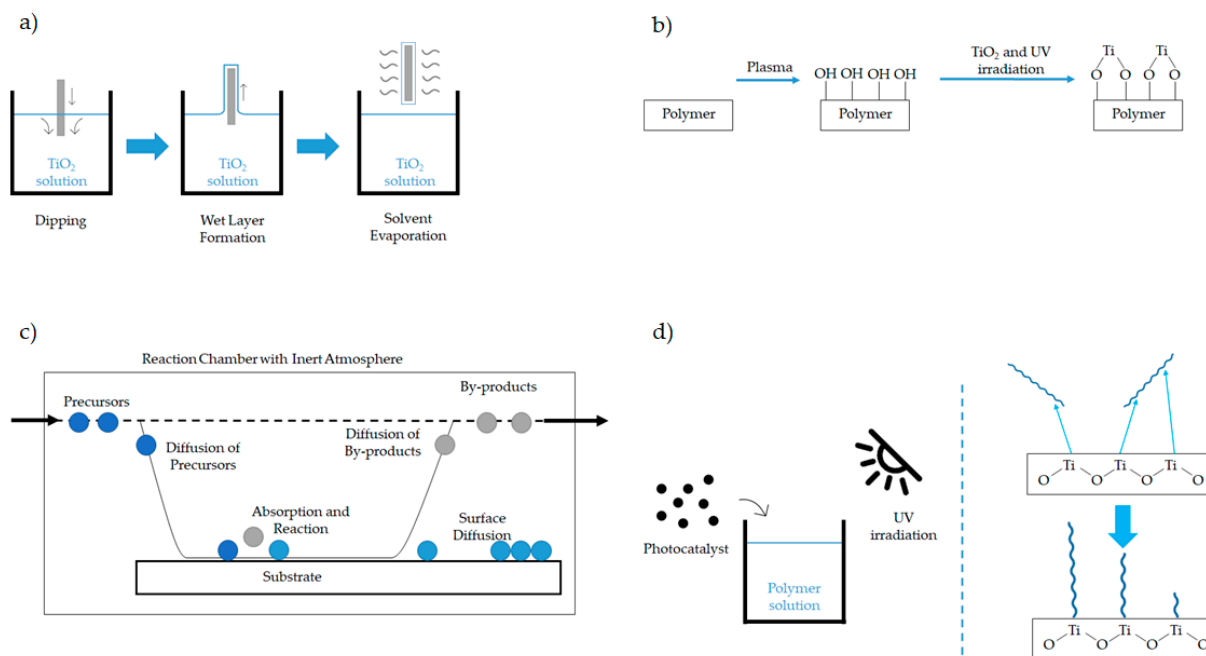


Figure 1. Schematic representation of the immobilization process on the surface by (a) dip-coating, (b) plasma treatment followed by UV irradiation, (c) chemical vapor deposition, and (d) grafting.

Plasma treatment provides many possibilities to refine a polymer surface, enabled by the adjustment of parameters such as gas flows, power, pressure, and treatment time [32]. The use of cold plasma enables modification of the surface characteristics to improve bonding without affecting bulk properties [33]. Plasma treatments of polymer surfaces cause not only a modification during the plasma exposure, but also leave active sites at the surfaces which are subject to post-reactions, which is desirable for later immobilization of the catalyst [32,34]. This is achieved using inert gases such as He, Ar, O₂, and N₂, because they are capable of inserting or substituting functional groups or creating radicals on the polymer surface, which enhance hydrophilicity or improve adhesion [35]. For example, after plasma activation in air, a great variety of different oxygen-containing functional groups, such as -OH, -C=O, and -COOH, are introduced onto the surface of the material [36]. The polymer can then be irradiated with ultraviolet light in the presence of the photocatalyst in order to immobilize it on the support [34], as illustrated in Figure 1b.

The catalyst can also be deposited on the polymer surface by the chemical vapor deposition (CVD) method, as shown in Figure 1c. During this process, a substrate is exposed to a single- or multi-component volatile precursor (in gaseous phase) in an inert atmosphere (N₂, Ar, or He) at controlled high temperature and pressure [37–39]. The precursors are vaporized and allowed to flow into the reaction chamber where a chemical reaction forms the desired photocatalytic material which is then deposited onto a support, driven by thermal energy [37,38,40]. Usually, by-products are also generated during this process and will be removed by flowing gas through the reactor [37].

Instead of immobilizing the catalyst on the polymer, the polymer can be deposited on the catalyst by grafting under UV light [41,42], as illustrated in Figure 1d. The grafting process can be understood as follows: (i) under light, the photocatalyst generate electron-hole pairs, which excite hydroxyl groups and water molecules on the surfaces; (ii) the activated molecules partially cleave the bonds of surrounding polymer; and (iii) these segmented chains form a covalent bond with the photocatalyst [41].

2.3.2. Immobilization in the Matrix

As for the immobilization in the matrix, this approach allows to reduce the photocatalyst leaching and offers other advantages, including low energy requirements and a better reusability [9]. However, drawbacks are also to be considered, such as the agglomeration of the photocatalyst inside the matrix [9]. This process can be carried out in situ or ex situ. In the ex situ process, the inorganic nanoparticles are first synthesized and then introduced into the polymer solution [43]. However, homogeneous dispersion is difficult to obtain, and the agglomerates formed are difficult to break [43,44]. To overcome this difficulty, the in situ approach can be used [43,44]. Here, the metal or metal oxide particles are generated inside the polymeric phase using a precursor metal [43,44].

Examples of in situ processes are in situ polymerization and sol–gel processes, which are illustrated in Figure 2a,b. In situ polymerization is a highly effective method of synthesis of polymer nanocomposites, which occurs “in the polymerization mixture” [45]. It involves the blending of a nanomaterial in a solution containing a neat monomer, followed by polymerization [45,46]. The sol–gel process is associated with two main reactions: hydrolysis and condensation (Equations (5) and (6)). During hydrolysis, cleavage of the bond occurs between the organic chain and the metal; consequently, its substitution by -OH groups takes place through nucleophilic addition [43,44]. During condensation, oxygen–metal–oxygen (-O-M-O-) bonds are formed and small molecules, such as water, are released [43,44]. The in situ formation of nanoparticles via sol–gel methods may occur either in the presence of a preformed polymer, or by the simultaneous formation of the organic network, forming an interpenetrating polymer network [44].

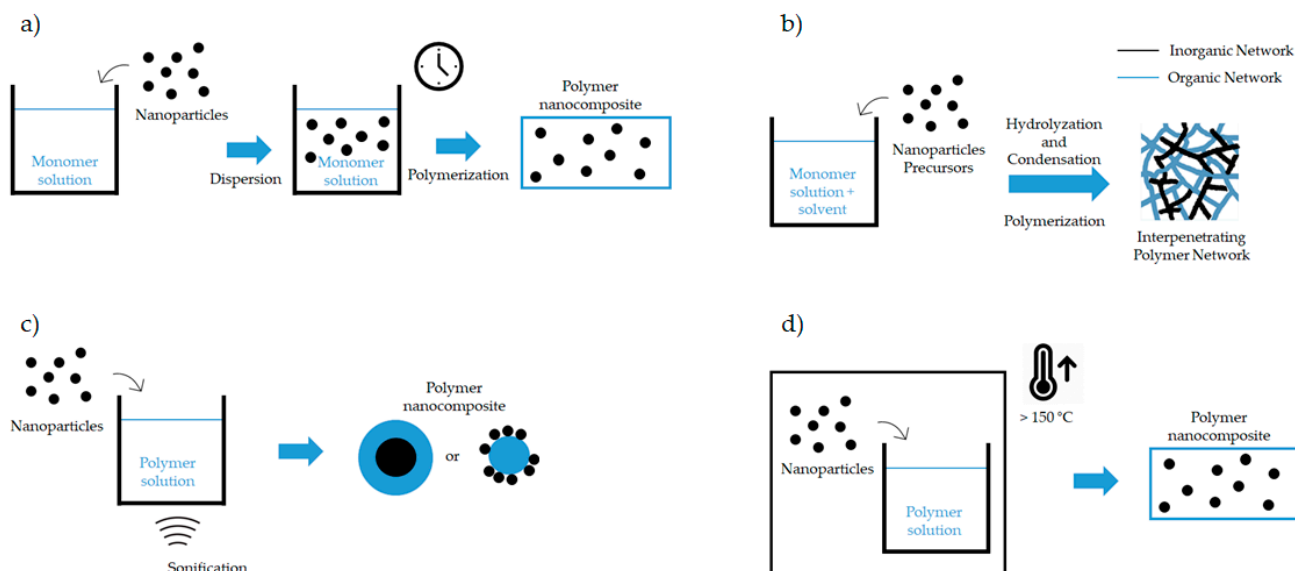
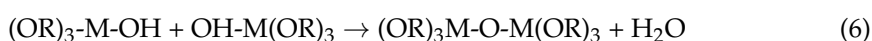
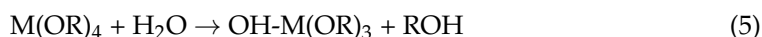


Figure 2. Schematic representation of the immobilization process on the matrix by (a) in situ polymerization, (b) sol–gel process, (c) mixing the catalyst and the polymer, (d) hydrothermal process.

Examples of ex situ processes are mixing the catalyst with a polymer and the hydrothermal process, which are illustrated in Figure 2c,d. During the direct mixing of the polymer with the catalyst nanoparticles, the polymer will cover the surface of the catalyst [45]. In this process, the dispersion of nanoparticles in the polymer matrix is a critical issue in the successful preparation of transparent hybrid nanocomposites; therefore, after mixing, sonication methods are applied to disperse the particles [46]. The hydrothermal

process is similar, because it involves mixing of the polymer and the catalyst, but it is performed at high temperatures [47,48].

2.4. Operation Parameters Effect

As in any process, during heterogeneous photocatalysis, special attention must be paid to the operational parameters, because these influence the characteristics of the composite, and consequently, the effectiveness of the photocatalysis. The operating conditions to consider are the composition of the composite (polymer charge and catalyst dosage), the pollutant concentration, the pH value of the medium, the radiation source, and the concentration of the composite introduced into the medium.

2.4.1. Polymer Load

The polymer load can affect the thickness of the composite [49–52], its light absorption capacity [49,53], the electron–hole pair recombination rate [49], the catalyst agglomeration [13,54,55], and the composite crystallinity [56].

Lee et al. [50], Zhao et al. [51], and Mohammed et al. [52] studied catalyst/polyaniline (PANI) composite powders for dye degradation. Lee et al. [50] evaluated the degradation of methylene blue (MB) and bisphenol A (BPA) with TiO₂/PANI composites, produced by mixing the polymer and the nanoparticles, with different PANI contents (2, 4, 6, 8, 10 wt.%). Zhao et al. [51] coated TiO₂ nanoparticles with different amounts of PANI by varying the aniline volume (1, 0.5, 0.25 mL) added to the polymerization medium and used the TiO₂/PANI powder to degrade rhodamine B (RhB). Mohammed et al. [52] synthesized a Cu₂O-ZnO/PANI ternary powder composite by in situ polymerization, with different amounts of PANI by varying the aniline volume (0.13, 0.10, 0.05, 0.03 mL) added to the polymerization medium. This composite was then used to remove Congo red dye (CR). Despite having immobilized different photocatalysts with different immobilization techniques, they all concluded that the increase in the amount of polymer results in a decrease in the efficiency of the process, due to the increase in the thickness of the material that prevents contact between the inner layer of the catalyst with oxygen, water, and contaminants. In addition, thick PANI layers can reduce the light absorption of the catalyst [53].

Asgari et al. [49] prepared a ZnO/PANI powder composite through in situ polymerization, to degrade metronidazole (MNZ). Different amounts of aniline (0.0392, 0.196, 0.392 mL) were added to the polymerization medium to obtain composites with varying amounts of PANI. Asgari et al. [49] also reported the two phenomena presented above and, in addition, it was also concluded that an initial increase in the PANI load induces an increase in the pollutant removal due to the suppression of e⁻/h⁺ pair recombination.

Saravanan et al. [55] added different amounts of PANI (1 M, 1.5 M, and 2 M) into the polymerization medium to create a ZnO/PANI powder, which was then used to degrade methyl orange (MO) and MB. Montallana et al. [13] dispersed TiO₂ nanoparticles in PVA solutions (8 and 12 wt.%) and produced a TiO₂/PVA film via electrospinning. It was reported that a higher PVA load led to a lower formation of agglomerates and higher surface areas, due to the existence of smaller surface tensions. Wang et al. [54] prepared a powder TiO₂/PVA composite through the hydrothermal method, with different feed ratios of PVA to TiO₂ (5, 10, 20, 40 wt.%), and used them to remove MO. It was concluded that when the PVA content exceeded 10% by weight, the surface tension ceased to decrease, and the agglomeration slightly increased.

El-Drafiawy et al. [56] prepared a ZnO/PVA powder composite, with different amounts of PVA to ZnO (5, 7, 10 wt.%), by the sol–gel method. This composite was used to remove MB and MO. It was concluded that an increase in the PVA load induced a decrease in the crystallinity degree, because PVA is a semi-crystalline material. It was also found that, depending on the pollutant, different ratios of PVA to ZnO are required to achieve the optimal performance.

The conditions tested in the studies discussed above, as well as the main results achieved, are presented in Table 1.

Table 1. Summary of studies that have analyzed the effect of the polymer load on the polymer-supported photocatalysis process.

Composite	Immobilization Technique	Conditions Tested	Results	Reference
TiO ₂ /PANI powder	Mixing	[BPA] ₀ = 5 mg/L [MB] ₀ = 5 μM 6 10.3 W/m ² visible light lamps <i>t</i> = 360 min PANI = {2, 4, 6, 8, 10} wt.%	4 wt.% PANI MB removal of 99% (<i>k</i> = 0.013 min ⁻¹) BPA removal of 80% (<i>k</i> = 0.004 min ⁻¹)	[50]
TiO ₂ /PANI powder	In situ polymerization	[RhB] ₀ = 10 mg/L 350 W/m ² Suntest lamp <i>t</i> = 70 min TiO ₂ /Aniline = {0.015, 0.03, 0.06} mg/mL	0.06 mgTiO ₂ /mL _{aniline} 90% removal (<i>k</i> = 0.033 min ⁻¹)	[51]
Cu ₂ O-ZnO/PANI powder	In situ polymerization	[CR] ₀ = 30 mg/L 100 W LED light pH = 6 <i>t</i> = 30 min Cu ₂ O-ZnO/Aniline = {33, 20, 10, 7.7} g/mL	10 gTiO ₂ /mL _{aniline} 95% removal (<i>k</i> = 0.10 min ⁻¹)	[52]
ZnO/PANI powder	In situ polymerization	[MBZ] ₀ = 10 mg/L 31 W/m ² UV lamp or 26.5 W/m ² xenon lamp pH = 7; <i>t</i> = 3 h ZnO/Aniline = {102, 20, 10} g/mL	20 gTiO ₂ /mL _{aniline} 97% removal <i>k</i> = 0.025 min ⁻¹ for visible <i>k</i> = 0.034 min ⁻¹ for UV	[49]
ZnO/PANI powder	Mixing	MO and MB 250 W visible lamp 1.5 M PANI <i>t</i> = 3 h	MO removal of 98.3% (<i>k</i> = 0.023 min ⁻¹) MB removal of 99.2% (<i>k</i> = 0.026 min ⁻¹)	[55]
TiO ₂ /PVA film	Mixing	[MB] ₀ = 2.5 ppm 5 6 W UV lamp 1 wt.% TiO ₂ <i>t</i> = 360 min Mix the TiO ₂ in an 8 wt.% PVA solution or in a 12 wt.%	12 wt.% PVA solution 70% removal (<i>k</i> = 0.003 min ⁻¹)	[13]
TiO ₂ /PVA powder	Hydrothermal Method	[MO] ₀ = 15 mg/L 600 W/m ² xenon lamp <i>t</i> = 50 min PVA = {5, 10, 20, 40} wt.%	40 wt.% PVA 95% removal (<i>k</i> = 0.060 min ⁻¹)	[54]
ZnO/PVA powder	Sol-gel	[MB] ₀ = 10 ppm 400 W halogen-mercury lamp <i>t</i> = 20 min PVA = {5, 7, 10} wt.%	5 wt.% PVA ~100% removal (<i>k</i> = 0.230 min ⁻¹)	[56]
		[MB] ₀ = 10 ppm 400 W halogen-mercury lamp <i>t</i> = 90 min PVA = {5, 7, 10} wt.%	7 wt.% PVA 70% removal (<i>k</i> = 0.013 min ⁻¹)	

From the analysis of the results obtained, it appears that, at least for cases in which PVA or PANI are used as a support, the efficiency of the process vs. the amount of polymer in the composite is given by a parabolic profile, as shown in Figure 3. For lower amounts of polymer, the formation of agglomerates is avoided and the effect of decreasing the recombination rate of e⁻/h⁺ is superimposed. However, for higher amounts of polymer, in addition to the formation of catalyst agglomerates, which causes a decrease in the surface area, the effect of increasing the composite thickness, and consequently, decreasing the light absorption, is dominant, leading to an efficiency decrease.

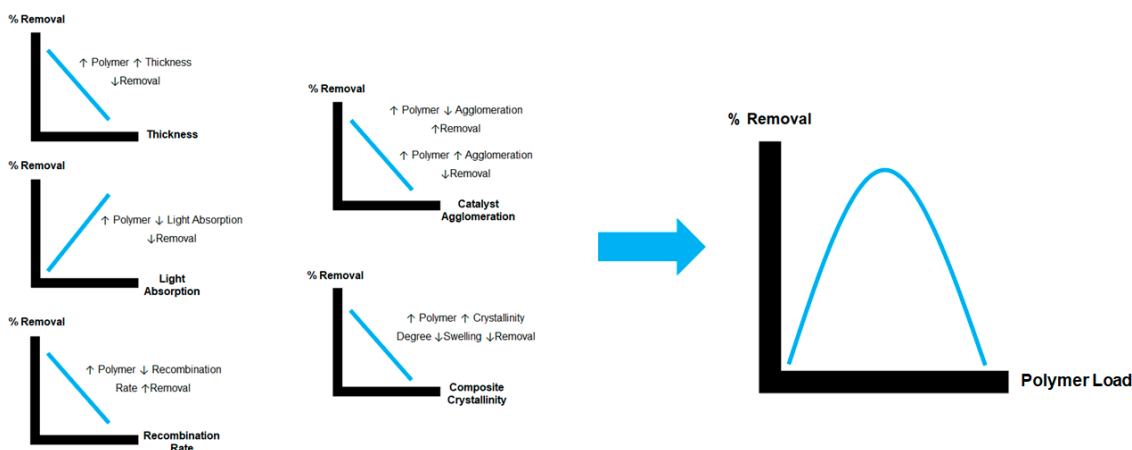


Figure 3. Effect of polymer addition on pollutant removal.

2.4.2. Photocatalyst Dosage

The catalyst dosage can influence the material crystallinity [57–59] and agglomeration [34,60–62], the composite contact angle [58,59], pore volume [63], and BG [57,64].

Khan et al. [58] and Lou et al. [59] prepared an $\text{Al}_2\text{O}_3\text{-ZnO/PVA}$ film and a $\text{TiO}_2\text{/PVA}$ film, respectively, by mixing the polymers with the catalysts. Lou et al. [59] analyzed the performance of films with 1, 3, 5, 10 and 20 wt.% $\text{TiO}_2\text{/PVA}$, and Khan et al. [58] evaluated the performance of 5, 7 and 9 wt.% $\text{Al}_2\text{O}_3\text{-ZnO/PVA}$ films, to degrade RhB and MB, respectively. It was concluded that an increase in the catalyst dosage provides an increase in the material crystallinity, and consequently, in its contact angle, due to a reduction in the water absorption capacity. These phenomena cause a reduction in the process efficiency.

Lei et al. [60] prepared a variety of $\text{TiO}_2\text{/PVA}$ films, with weight ratios of TiO_2 to PVA of 1, 3, 5, 7, 10, and 12 wt.%, by mixing PVA on a TiO_2 solution. Wang et al. [61] mixed various amounts of nanoparticles with polydimethylsiloxane (PDMS) to create $\text{TiO}_2\text{/PDMS}$ films with different mass ratios of TiO_2 to PDMS (25, 50, 75, 100, 125 wt.%). Gomes et al. [34] synthesized $\text{TiO}_2\text{/PDMS}$ films with different amounts of TiO_2 by submerging plasma-treated PDMS films in TiO_2 solutions, under UV light (70, 140, 280, 1000, 10,000 mg/L). Hossain and Chun [62] prepared ZnO/PDMS sponges with different amounts of ZnO (200, 600, 1000 mg), using the sugar template method. These composites were used to degrade MO, MB, and parabens (methylparaben, MP; ethylparaben, EP; and propylparaben, PPP). According to these studies, the effect of the catalyst load on the surface area exhibits a parabolic behavior. Beyond the optimal value, an increase in the catalyst concentration no longer results in a decrease in the surface tension; consequently, the agglomeration increases and the surface area decreases.

Hickman et al. [63] fabricated $\text{TiO}_2\text{/PDMS}$ sponges with different amounts of catalyst (36, 71 and 142 $\mu\text{g/g}_{\text{sponge}}$), using the sugar template method. The photocatalytic activity was analyzed by RhB degradation. It was concluded that increasing the catalyst amount causes a reduction in material pore size. Thus, despite the decrease in the amount of pollutant absorbed, the reaction kinetic is higher, and consequently, more pollutant is degraded.

Vijayalakshmi et al. [64] and Sahu et al. [57] prepared a ZnO/PANI powder through in situ polymerization. These composites were later used to remove MB, under sunlight and UV irradiation. It was observed that increasing the amount of catalyst, from 1 wt.% to 10 wt.%, resulted in a decrease in the composite BG from 2.19 to 2.10 eV [64]. A further increase from 10 wt.% to 30 wt.% induced an increase in the nanocomposite BG from 2.00 to 2.07 eV [57]. The aforementioned studies had different conclusions. Vijayalakshmi et al. [64] concluded that the addition of ZnO increases the material conductivity, consequently decreasing its BG; Sahu et al. [57] verified the opposite. This phenomenon may be justified by the polymerization media composition, because Vijayalakshmi et al. [64] used 2 M

HCl to acidify it and Sahu et al. [57] opted for 0.15 M orthophosphoric acid, which led to the production of PANI with different BG values (2.30 eV and 1.96 eV, respectively). An excessive amount of ZnO disorders the structure of the PANI chain, by overlapping unpaired free electrons in the localized polaron; therefore, the charge carriers present in the composite are unable to move freely, which reduces the conductivity [64]. Perhaps the percentages of ZnO which are classified as excessive are dependent on the polymerization media composition.

Table 2 summarizes the studies discussed before, as well as the key operating conditions and results. Notably, only the first two studies analyzed variations in the material's BG, meaning that values of this characteristic are not mentioned for the other studies.

Table 2. Summary of studies that have analyzed the effect of the photocatalyst dosage on the polymer-supported photocatalysis process.

Composite	Immobilization Technique	Conditions Tested	Results	Reference
ZnO/PANI powder	In situ polymerization	[MB] ₀ = 10 ppm Natural irradiation <i>t</i> = 160 min ZnO = {1, 10} wt.%	10 wt.% ZnO BG = 2.10 eV 91% removal (<i>k</i> = 0.015 min ⁻¹)	[64]
ZnO/PANI powder	In situ polymerization	[MB] ₀ = 0.01 mg/L 8 W UV lamp <i>t</i> = 75 min ZnO = {10, 20, 30} wt.%	30 wt.% ZnO BG = 2.07 eV 57% removal (<i>k</i> = 0.011 min ⁻¹)	[57]
TiO ₂ /PVA film	Mixing	[RhB] ₀ = 10 ppm 18 W LED lamp <i>t</i> = 49 d TiO ₂ = {1, 3, 5, 10, 20} wt.%	10 wt.% TiO ₂ 80% removal (<i>k</i> = 2.2 × 10 ⁻⁵ min ⁻¹)	[59]
TiO ₂ /PVA film	Mixing	[MO] ₀ = 15 mg/L 6 0.9 W/m ² UV lamp 10 wt.% TiO ₂ <i>t</i> = 5 h TiO ₂ = {1, 3, 5, 10, 12} wt.%	10 wt.% TiO ₂ ~100% removal (<i>k</i> = 0.015 min ⁻¹)	[60]
Al ₂ O ₃ -ZnO/PVA powder	Mixing	[MB] ₀ = 5 mg/L Solar radiation <i>t</i> = 30 min ZnO = {5, 7, 9} wt.%	9 wt.% ZnO 100% removal (<i>k</i> = 0.15 min ⁻¹)	[58]
TiO ₂ /PDMS film	Plasma Treatment + UV Irradiation	[MP] ₀ = [EP] ₀ = [PPP] ₀ = 1 mg/L Solar radiation 680 ± 150 W/m ² <i>t</i> = 2 h TiO ₂ = {70, 140, 280, 1000, 10,000} mg/L	140 mg/L MP removal of ~23% EP removal of ~27% PPP removal of ~33%	[34]
TiO ₂ /PDMS film	Mixing	[MB] ₀ = 0.01 m M Solar radiation <i>t</i> = 6 d TiO ₂ = {25, 50, 75, 100, 125} wt.%	75 wt.% TiO ₂ ~100% removal (<i>k</i> = 0.001 min ⁻¹)	[61]
	Mixing	Oleic Acid 48 W mercury lamp <i>t</i> = 30 min TiO ₂ = {25, 50, 75, 100, 125} wt.%	75 wt.% TiO ₂ ~100% removal (<i>k</i> = 0.15 min ⁻¹)	

Table 2. Cont.

Composite	Immobilization Technique	Conditions Tested	Results	Reference
TiO ₂ /PDMS sponges	Sugar Template	[RhB] ₀ = 5 mg/L 1000 W/m ² xenon lamp <i>t</i> = 1 h TiO ₂ = {36, 71, 142} µg/g _{sponge}	71 µgTiO ₂ /mg _{sponge} 80% removal (<i>k</i> = 0.027 min ⁻¹)	[63]
ZnO/PDMS sponges	Sugar Template	[MB] ₀ = 5 ppm 100 W halogen lamp or 4 W UV lamp <i>t</i> = 3 h ZnO = {200, 600, 1000} mg/sponge	600 mg ZnO 85% removal with halogen lamp (<i>k</i> = 0.0094 min ⁻¹) 73% removal with UV lamp (<i>k</i> = 0.007 min ⁻¹)	[62]

Based on the obtained results, it seems that the efficiency of the process vs. amount of catalyst in the composite shows a parabolic profile, as illustrated in Figure 4. For lower amounts of catalyst, the formation of agglomerates is avoided, and in the case of PVA, the swelling capacity is higher. However, for higher amounts of catalyst, in addition to the forming of catalyst agglomerates, which causes a decrease in the surface area, the increase in the degree of crystallinity causes a reduction in the swelling ability for the PVA films.

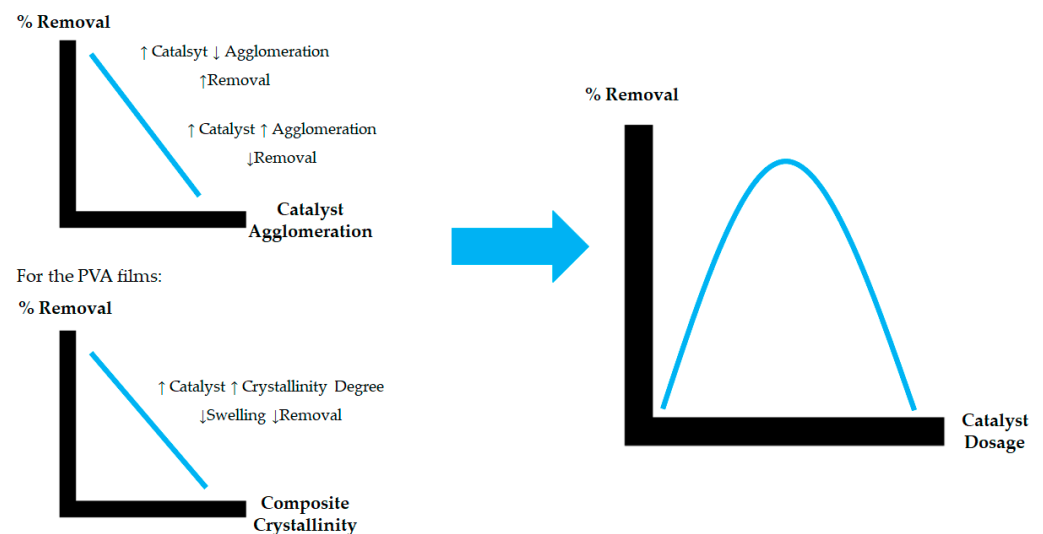


Figure 4. Effect of photocatalyst addition on pollutant removal.

From the studies that optimized the photocatalytic oxidation process in terms of the catalyst load present in the composite films, it was concluded that the most favorable value for the catalyst/polymer mass ratio is 10% for PVA films. In the case of catalyst/PDMS films, a greater amount of catalyst in relation to the amount of polymer (75 wt.%) seems to be necessary to achieve significant removal of the pollutants.

2.4.3. pH Value

The pH value affects the adsorption–desorption of the organic molecules on the surface of the photocatalyst [47,65–67], the generation of hydroxyl radicals and active oxygen species [52,65,67], and the composite stability [68].

Mohammed et al. [52] synthesized a Cu₂O-ZnO/PANI ternary powder composite through in situ polymerization. This composite was then used to remove CR from solutions with different pHs (3, 6, and 9). According to this study and those mentioned above, at a

lower pH, holes are considered major contributors to the photocatalytic activity, whereas at neutral or high pH, hydroxyl radicals are believed to be the major oxidant moieties. The pH value also influences the attraction between the catalyst and the molecules of water that will form OH^\bullet .

Ghule et al. [65] evaluated the effect of the pH (3, 5, 7, 10, and 12) on the degradation of MO by a ZnO/PVA powder prepared by mixing the polymer with the catalyst. Yan et al. [47] used TiO_2 /PVA films, synthesized by the hydrothermal method, to remove Cr(VI) from solutions with different pHs (1.8, 2.2, 3, 3.9, 4.2, 5.9, and 6.4). Chen et al. [66] used CeO_2 - TiO_2 /PANI films, created by an electrochemical method, to remove tetrabromobisphenol A (TBBPA) from reaction media with different pHs (1, 3, 5, 7, and 9). Sambaza et al. [67] prepared a TiO_2 /PANI powder using in situ polymerization, to degrade BPA, and evaluated the pH effect in this process by varying it (4, 6.5, 7, and 10). Regardless of the composite used and its method of preparation, the studies found that the best pH value depends on the zero-point charge (pHzpc) of the composite and on the characteristics of the pollutant, to induce an electrostatic attraction between them. For example, basic dyes, such as MB and methyl green (MG), are positively charged, whereas acid dyes, such as MO and CR, are negatively charged. Therefore, to remove basic dyes from the water, a pH higher than the pHzpc of the catalyst must be selected, and to remove the azo dyes, a pH lower than the pHzpc must be chosen. According to the literature, the pHzpc of TiO_2 is 6.3 and that of ZnO is 9 [65,67]. However, Azeez et al. [69] reported that pHzpc may depend on the conditions used during preparation of the nanoparticles.

Ren et al. [68] prepared TiO_2 /PVA films by mixing the polymer and the nanoparticles. This composite was used to remove bezafibrate (BZF) from solutions with different pHs (4.2, 6.9, and 9.2). It was concluded that at lower pH values, the Ti-O-C bonds can be destroyed, which results in the release of TiO_2 into the solution; in addition, at lower pHs, the degradative effect of the catalyst on PVA is more significant. Therefore, in acidic conditions, the mass loss of catalyst/PVA is larger (15%) than in neutral (10%) or basic media (<1%).

Thus, the best pH value is a compromise between the non-degradation of the composite, the generation of radicals, and a good electrostatic attraction between the pollutant and the catalyst. Table 3 resumes the main results discussed in the literature regarding the effect of pH on the heterogeneous photocatalytic oxidation of pollutants using polymeric composites.

Table 3. Summary of studies that have analyzed the effect of the pH value on the polymer-supported photocatalysis process.

Composite	Immobilization Technique	Conditions Tested	Results	Reference
ZnO/PVA powder	Mixing	[MO] ₀ = 20 mg/L T = 27 °C 400 kW/m ² mercury lamp 8 wt.% ZnO t = 80 min pH = {3, 5, 7, 10, 12}	pH = 7 95% removal (k = 0.05 min ⁻¹)	[65]
TiO ₂ /PVA films	Hydrothermal method	[Cr(VI)] ₀ = 10 ppm 1 W/m ² xenon lamp or 5 W/m ² UV lamp or 1.05 W/m ² solar irradiation 20 wt.% TiO ₂ t = 25 min pH = {1.8, 2.2, 3, 3.9, 4.2, 5.9, 6.4}	pH = 3.9 UV and solar: 100% removal (k = 0.18 min ⁻¹) Xenon lamp: 90% removal (k = 0.09 min ⁻¹)	[47]

Table 3. Cont.

Composite	Immobilization Technique	Conditions Tested	Results	Reference
CeO ₂ -TiO ₂ /PANI films	Galvanostatic	[TBBPA] ₀ = 10 mg/L 1200 W/m ² xenon lamp <i>t</i> = 120 min pH = {1, 3, 5, 7, 9}	pH = 3 96% removal (<i>k</i> = 0.027 min ⁻¹)	[66]
TiO ₂ /PANI powder	In situ polymerization	[BPA] ₀ = 5 ppm UV lamp <i>t</i> = 80 min pH = {4, 6.5, 7, 10}	pH = 10 99.7% removal (<i>k</i> = 0.046 min ⁻¹)	[67]
Cu ₂ O-ZnO/PANI powder	In situ polymerization	[CR] ₀ = 30 mg/L 100 W LED light Cu ₂ O-ZnO/Aniline = 10 g/mL <i>t</i> = 30 min pH = {3, 6, 9}	pH = 6 95% removal (<i>k</i> = 0.10 min ⁻¹)	[52]
TiO ₂ /PVA films	Mixing	[BZF] ₀ = 10 mg/L 11 wt.% TiO ₂ Solar simulator 1 kW <i>t</i> = 60 min pH = {4.2, 6.9 and 9.2}	pH = 6.9 15% removal (<i>k</i> = 0.003 min ⁻¹)	[68]

2.4.4. Composite Load

As mentioned by Lee et al. [50], Mohammed et al. [52], Olad and Nosrati [70], Sharma et al. [71], and Habtamu et al. [72], there is an optimal point for the amount of composite to be introduced into the reaction medium. Different catalysts were applied in all these studies to degrade different pollutants, although all were supported on the same polymer; however, the same conclusion was drawn. When the catalyst dosage is inferior to the optimal point, there are fewer active sites available on the catalyst surface, which, subsequently, leads to lower light absorption, and finally leads to reduced photocatalytic activity. Similarly, when the composite dosage is higher than the optimal value, there is an increase in the turbidity of the solution [70,72]. Increasing the turbidity prevents light transmission and increases its scattering [70,72]. In addition, increasing the amount of composite can also cause agglomeration, which will reduce the amount of surface exposed to radiation and decrease the penetration depth of light, causing scattering, which lowers the light intensity entering the suspension [50,52,71]. Both phenomena affect light penetration and impede the catalyst activation, which ultimately decreases the degradation rate. The conditions tested in these studies and the results are presented in Table 4.

Table 4. Summary of studies that have analyzed the effect of the composite load on the polymer-supported photocatalysis process.

Composite	Immobilization Technique	Conditions Tested	Results	Reference
ZnO/PANI powder	In situ polymerization	[MB] ₀ = 10 mg/L ZnO/Aniline = 46.5 mg/mL 30 W UV lamp and 50 W halogen lamp with UV filter <i>t</i> = 1 h [composite] = {0.75, 1.5, 2} g/L	1.5 g/L composite UV: 28% removal (<i>k</i> = 0.005 min ⁻¹) Visible: 82% removal (<i>k</i> = 0.029 min ⁻¹)	[70]

Table 4. Cont.

Composite	Immobilization Technique	Conditions Tested	Results	Reference
TiO ₂ /PANI powder	In situ polymerization	[BPA] ₀ = 5 mg/L [MB] ₀ = 5 µM 6 10.3 W/m ² visible light lamps <i>t</i> = 360 min 4 wt.% PANI [composite] = {0.3, 0.7, 1.2, 1.7} g/L	1.2 g/L composite MB removal of 99% (<i>k</i> = 0.013 min ⁻¹) BPA removal of 80% (<i>k</i> = 0.004 min ⁻¹)	[50]
FeO-ZnO/PANI powder	In situ polymerization	[3-APh] ₀ = 10 mg/L Sunlight <i>t</i> = 120 min [composite] = {20, 40, 60, 80, 100} mg/L	80 mg/L composite 92% removal (<i>k</i> = 0.021 min ⁻¹)	[71]
Ag-ZnO/PANI powder	In situ polymerization	[MG] ₀ = 200 mg/L Visible light <i>t</i> = 120 min pH = 8 [composite] = {0.1, 0.2, 0.3, 0.4} g/L	0.2 g/L composite 98.6% removal (<i>k</i> = 0.036 min ⁻¹)	[72]
Cu ₂ O-ZnO/PANI powder	In situ polymerization	[CR] ₀ = 30 mg/L 100 W LED light Cu ₂ O-ZnO/Aniline = 10 g/mL <i>t</i> = 30 min pH = 6 [composite] = {0.05, 0.1, 0.15} g/L	0.05 g/L composite 95% removal (<i>k</i> = 0.10 min ⁻¹)	[52]

2.4.5. Pollutant Concentration

The effect of the pollutant concentration on the process efficiency was evaluated by Asgari et al. [49], Mohammed et al. [52], Hickman et al. [63], Sambaza et al. [67], Habtamu et al. [72], and Lian et al. [73]. Hickman et al. [63] prepared PDMS sponges by the sugar template method, and injected these with TiO₂ solutions. These sponges were used to degraded different solution of RhB (2.5, 5, 10 mg/L). Asgari et al. [49], Sambaza et al. [67], Habtamu et al. [72], and Mohamed used in situ polymerization to synthesize ZnO/PANI, TiO₂/PANI, Ag-ZnO/PANI, and Cu₂O-ZnO/PANI powders, respectively. These were used to degraded MNZ (10, 20, 30, 40 mg/L), BPA (1, 5, 10, 15, 20, 30 ppm), MG (0.1, 0.2, 0.3, 0.4, 0.5 g/L), and CR (30, 50, 80 mg/L), respectively. Lian et al. [73] synthesized C-TiO₂/PDMS particles by mixing C-TiO₂, previously prepared using the sol-gel method, with PDMS and used them to remove different amounts of RhB (4, 7, 10, 13, 16, 19 mg/L), from aqueous solutions. Table 5 presents the conditions tested and the results of these studies.

It was reported that, initially, an increase in the pollutant concentration may induce an increase in pollutant removal. This phenomenon is due to an increase in the driving force that promotes the transfer of pollutant from the solution to the composite. However, the excessive increase does not improve the process efficiency, because the number of active sites is limited [63,73], and it can block the passage of light and cause a reduction in the photons that can reach the composite surface; therefore, fewer OH• radicals are generated [52,67,72].

Table 5. Summary of studies that have analyzed the effect of the composite load on the polymer-supported photocatalysis process.

Composite	Immobilization Technique	Conditions Tested	Results	Reference
TiO ₂ /PDMS sponge	Sugar Template	[RhB] ₀ = {2.5, 5, 10} mg/L 71 µgTiO ₂ /mg sponge 1000 W/m ² xenon lamp t = 1 h	[RhB] ₀ = 5 mg/L 80% removal (k = 0.027 min ⁻¹)	[63]
C-TiO ₂ /PDMS	Mixing	[RhB] ₀ = {4, 7, 10, 13, 16, 19} mg/L 500 W UV lamp pH = 3 t = 3 h	[RhB] ₀ = 13 mg/L 86% removal (k = 0.011 min ⁻¹)	[73]
TiO ₂ /PANI powder	In situ polymerization	[BPA] ₀ = {1, 5, 10, 15, 20, 30} ppm UV lamp pH = 10 t = 80 min	[BPA] ₀ = 5 ppm 99.7% removal (k = 0.046 min ⁻¹)	[67]
ZnO/PANI powder	In situ polymerization	[MBZ] ₀ = {10, 20, 30, 40} mg/L 31 W/m ² UV lamp or 26.5 W/m ² xenon lamp pH = 7 t = 3 h ZnO/Aniline = 20 g/mL	[MBZ] ₀ = 10 mg/L 97% removal k = 0.025 min ⁻¹ for visible k = 0.034 min ⁻¹ for UV	[49]
Ag-ZnO/PANI powder	In situ polymerization	[MG] ₀ = {0.1, 0.2, 0.3, 0.4, 0.5} g/L Visible light t = 120 min pH = 8	[MG] ₀ = 0.2 g/L 98.6% removal (k = 0.036 min ⁻¹)	[72]
Cu ₂ O-ZnO/PANI powder	In situ polymerization	[CR] ₀ = {30, 50, 80} mg/L 100 W LED light Cu ₂ O-ZnO/Aniline = 10 g/mL t = 30 min pH = 6	[CR] ₀ = 30 mg/L 95% removal (k = 0.10 min ⁻¹)	[52]

2.4.6. Radiation Source and Intensity

The radiation source and its intensity play key roles in the photocatalytic process. It is necessary for the incident light to have an energy greater than the material's BG for electron-hole pairs to form [13,14]. The BG of metal oxides, such as TiO₂ and ZnO, is known; however, when supported on polymeric materials, some modifications may occur as illustrated in Table 6.

The BG of the material obtained from the catalyst placement on different polymeric supports varies; thus, several researchers have analyzed the influence of different types of radiation on photocatalysis. The results of these studies are shown in Table 7.

Table 6. Band gap values for different catalytic materials.

Metal Oxide	BG (eV)	Composite	BG (eV)	Reference
-	-	ZnO/PVA	3.11	[74]
TiO ₂	3.24	Ag-TiO ₂ /PANI	3.00	[75]
TiO ₂	3.20	TiO ₂ /PANI	3.10	[67]
ZnO	3.21	ZnO/PANI	2.67	[55]
ZnO	3.10	ZnO/PANI	2.81	[49]
-	-	ZnO/PANI	2.10	[64]
-	-	ZnO/PANI	2.07	[57]
-	-	Ag-ZnO/PANI	2.61	[72]

Table 7. Summary of studies that have analyzed the effect of the radiation source on the polymer-supported photocatalysis process.

Composite	Immobilization Technique	Conditions Tested	Results	Reference
Ag-TiO ₂ /PANI	In situ polymerization	[BPA] ₀ = 5 mg/L 400 W UV lamp or 500 W halogen lamp <i>t</i> = 55 min for UV lamp and 110 min for halogen lamp	UV lamp: 99.5 % removal (<i>k</i> = 0.096 min ⁻¹) Halogen lamp: 99.7% removal (<i>k</i> = 0.053 min ⁻¹)	[75]
ZnO/PANI powder	In situ polymerization	[MB] ₀ = 10 mg/L ZnO/Aniline = 46.5 mg/mL 30 W UV lamp and 50 W halogen lamp with UV filter <i>t</i> = 1 h	UV lamp: 28% removal (<i>k</i> = 0.005 min ⁻¹) Halogen lamp: 82% removal (<i>k</i> = 0.029 min ⁻¹)	[70]
ZnO/PANI powder	In situ polymerization	[MB] ₀ = [MG] ₀ = 10 ⁻⁵ M 15 W UV lamp and solar irradiation <i>t</i> = 5 h for solar irradiation and 9 h for UV irradiation	Solar irradiation: 99% removal of both dyes (<i>k</i> = 0.015 min ⁻¹) UV irradiation: MB removal of 80% (<i>k</i> = 0.003 min ⁻¹) MG removal of 90% (<i>k</i> = 0.004 min ⁻¹)	[76]
ZnO/PANI powder	In situ polymerization	[MBZ] ₀ = 10 mg/L 31 W/m ² UV lamp or 26.5 W/m ² xenon lamp <i>t</i> = 3 h	UV lamp: 97% removal (<i>k</i> = 0.034 min ⁻¹) Xenon lamp: 97% removal (<i>k</i> = 0.025 min ⁻¹)	[49]
TiO ₂ /PVA films	Hydrothermal method	[Cr(VI)] ₀ = 10 ppm 1 W/m ² xenon lamp or 5 W/m ² UV lamp or 1.05 W/m ² solar irradiation <i>t</i> = 25 min	UV and solar radiation: 100% removal (<i>k</i> = 0.18 min ⁻¹) Xenon lamp: 90% removal (<i>k</i> = 0.09 min ⁻¹)	[47]

Table 7. Cont.

Composite	Immobilization Technique	Conditions Tested	Results	Reference
ZnO/PDMS sponges	Sugar Template	[MB] ₀ = 5 ppm 100 W halogen lamp or 4 W UV lamp <i>t</i> = 3 h	Halogen lamp: 85% removal (<i>k</i> = 0.0094 min ⁻¹) UV lamp: 73% removal (<i>k</i> = 0.007 min ⁻¹)	[62]
ZnO/PDMS films	Calatyls Deposition	[phenol] = 1 ppm 18 W luminescent lamp with or without a UV filter <i>t</i> = 30 h for UV light or 50 h for visible light	UV light: 96% removal (<i>k</i> = 1.8 × 10 ⁻³ min ⁻¹) Visible light: 93.9% removal (<i>k</i> = 9.3 × 10 ⁻⁴ min ⁻¹)	[77]
TiO ₂ /PDMS sponge	Sugar Template	[RhB] ₀ = 20 μM 20 mW UV light or 20 mW LED lamp <i>t</i> = 3 h for UV lamp or 5 h for LED lamp	UV lamp: 90% removal (<i>k</i> = 0.013 min ⁻¹) LED lamp: 10% removal (<i>k</i> = 3.5 × 10 ⁻⁴ min ⁻¹)	[78]

From the analysis of Table 6, it can be seen that the materials composed of polyaniline have lower BG than the others; therefore, with these materials, it is expectable to achieve higher reaction kinetics using the photocatalytic process under visible radiation. In fact, Olad and Nosrati [70], Eskizeybek et al. [76], and Asgari et al. [49] found that, under visible light, the PANI materials achieved higher or similar reaction kinetics. It should be noted that, under UV radiation, the same removal efficiencies were achieved, but the process was longer. Unexpectedly, Sambaza et al. [75] reported that the degradation of BPA took longer to achieve maximum degradation under visible light than under UV light, although the material had a higher absorption peak for wavelengths in the visible range.

The immobilization of catalysts in other polymers does not seem to significantly affect the material BG. Hossain and Chun [62], Sosnin et al. [77], and Lee et al. [78] prepared PDMS composites incorporated with a catalyst. These materials were later used to degrade MB, phenol, and Rhodamine B (RB), under UV, UV-visible and visible radiation. Hossain and Chun [62] found that the best radiation source was the UV-visible lamp, followed by the visible and UV lamps, which was unexpected because ZnO exhibits a high BG. In this study, no physical-chemical characterization tests were performed that could justify the obtained results. Yan et al. [47] also concluded that the photoreduction rate of Cr(VI) under outdoor sunlight irradiation was close to that under UV light irradiation, although the intensity of sunlight (1.05 W/m²) was much lower than that of the UV lamp (5 W/m²). The material also demonstrated good photocatalytic activity under visible light (1 W/m²) due to the shift in the absorption edge to the visible light region caused by the hydrothermal process. In contrast, both Sosnin et al. [77] and Lee et al. [78] reported that the decomposition rate under UV light was noticeably higher, as is generally expected, given the catalyst's large BG and the TiO₂/PDMS absorbance spectra, whereas it was near-constant in the dark and under visible light.

From the results of the studies mentioned above, it can be concluded that the best radiation source is dependent on the BG of the material. It is also verified that this characteristic is modified depending on the polymer used as a support, the composition of the material, and the treatment/immobilization process applied.

As previously mentioned, in addition to the radiation source, its intensity also plays a key role in the efficiency of the photocatalytic process, as shown in Table 8. Lei et al. [60] and Ghule et al. [65] degraded the same amount of MO, under UV lamps with different intensities, and, as expected, higher removal was achieved while using the lamp with the highest intensity. However, between these investigations, different catalysts were used, which can influence the results. However, Song et al. [79] and Yang et al. [80] degraded the same amount of RhB with the same catalyst, under similar light intensities conditions and, as expected, obtained similar kinetic reactions. Gomes et al. [34] evaluated the degradation of different parabens by TiO₂/PDMS films, under natural solar light at different times of the year, and concluded that, as expected, the experiments performed in June ($710 \pm 220 \text{ W/m}^2$) led to better removal of the paraben's mixture compared with the results obtained during October ($680 \pm 150 \text{ W/m}^2$).

Table 8. Summary of studies that have analyzed the effect of the radiation intensity on the polymer-supported photocatalysis process.

Composite	Immobilization Technique	Conditions Tested	Results	Reference
TiO ₂ /PVA films and ZnO/PVA powder	Mixing	[MO] ₀ = 15 mg/L $6 \times 0.9 \text{ W/m}^2$ UV lamps $t = 5 \text{ h}$ [MO] ₀ = 20 mg/L 400 Kw/m^2 $t = 90 \text{ min}$	90% removal ($k = 0.0076 \text{ min}^{-1}$) ~100% removal ($k = 0.051 \text{ min}^{-1}$)	[60,65]
C-TiO ₂ /PVA and TiO ₂ /PVA	Mixing	[RhB] ₀ = 10 mg/L 600 W/m^2 Visible lamp $t = 6 \text{ h}$ [RhB] ₀ = 10 mg/L 700 W/m^2 tungsten-halogen lamp $t = 6 \text{ h}$	90% removal ($k = 0.0064 \text{ min}^{-1}$) 89% removal ($k = 0.061 \text{ min}^{-1}$)	[79,80]
TiO ₂ /PDMS film	Plasma Treatment + UV Irradiation	[MP] ₀ = [EP] ₀ = [PPP] ₀ = 1 mg/L Solar radiation $680 \pm 150 \text{ W/m}^2$ or $710 \pm 220 \text{ W/m}^2$ $t = 2 \text{ h}$	$680 \pm 150 \text{ W/m}^2$: MP removal of ~23% EP removal of ~27% $710 \pm 220 \text{ W/m}^2$: MP removal of ~50% EP removal of ~53% PPP removal of ~33%	[34]

3. Recent Advances in Polymer-Supported Photocatalysis

The first study that boosted the research of polymer-supported photocatalysis was conducted by Tennakone et al. [81]. They supported TiO₂ on polythene (PE) films with thermal treatment to remove phenols from the water, under both UV and solar irradiation. Since then, other polymers, such as polypropylene (PP), polyethylene terephthalate (PET), PVA, PDMS, and PANI, associated with catalysts such as ZnO and TiO₂, have been analyzed.

Recently more attention has been given to:

- PANI, which is a conducting polymer and therefore works as a sensitizer to extend the spectral response of TiO₂ and ZnO to visible light [15,50];
- PVA, which possesses hydroxyl groups that form chemical bonds with the hydroxyl groups on the surface of inorganic nanoparticles [60];

- PMDS, because it is constituted of Si-O bonds, which make it resistant to the photooxidative effect of TiO₂, unlike polymers consisting of C-C bonds [82];
- Plastic wastes, such as PET bottles and PET or polystyrene (PS) food containers, to revalue a residue [83].

In the following sections, the characteristics of these supports, as well as the main results obtained in the photocatalytic oxidation of pollutants, will be discussed.

3.1. PANI-Supported Photocatalysis

Conducting polymers with narrow BGs enable the absorption of visible light from the sun. However, most conducting polymers exhibit a low mechanical strength and high brittleness [15]. Nevertheless, when combined with metal oxides, these limitations are overcome [15]. These exhibit a high photo response and possess a higher surface area, allowing for visible light absorption, low recombination of charge carriers, and high photocatalytic performance [15,50]. Namely, PANI has a prolonged alternate σ and π bond electronic cloud system, resulting in an energy BG of 2.8 eV [15,50]. When irradiated by ultraviolet–visible radiation (UV–Vis) and UV light, PANI can work as an extraordinary electron donor and hole acceptor photosensitizer [15,84].

As illustrated in Figure 5, TiO₂ and ZnO match well with PANI. The metal oxide conduction band (CB) is lower than the lowest unoccupied molecular orbital (LUMO) of PANI. Thus, the catalyst works as a sink for photogenerated electrons. The highest occupied molecular orbital (HOMO) of PANI is higher than the valence band (VB) of the metal oxide; thus, PANI can act as an acceptor for photogenerated holes [15,84]. Thus, a certain fraction of the holes and electrons of PANI is separated, reducing the change in recombination, and thereby enhancing the change in photocatalytic activity [72].

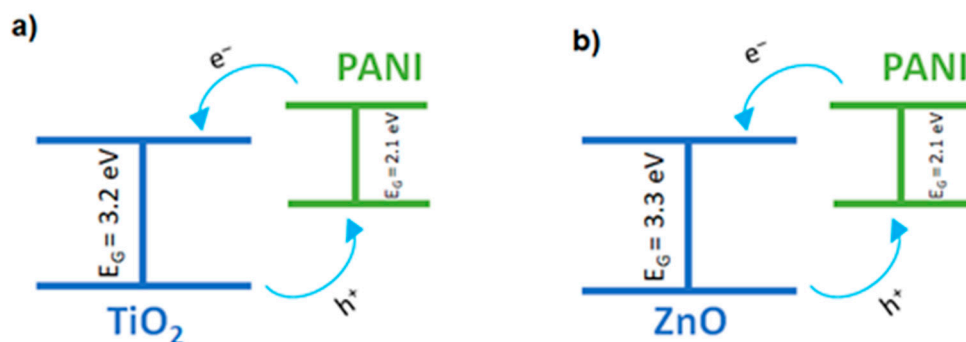


Figure 5. Schematic energy diagram for the composite of (a) PANI/TiO₂ and (b) PANI/ZnO.

Although the use of conducting polymers enables the use of visible radiation during the photocatalytic process, some researchers have also chosen to dope the catalyst to further reduce its BG. The catalyst surface modification effect was studied by Mohammed et al. [52], Brooms et al. [53], Sharma et al. [71], Habtamu et al. [72], Wahyuni et al. [85], and Sambaza et al. [75]. This method is used to extend the spectral response of the catalyst to visible light and to enhance the separation of photogenerated charges, and can be performed using non-metals such as nitrogen, carbon, and sulfur, or noble metals such as silver, gold, and copper [14,16,75]. The results of these studies are presented in Table 9.

Some of the studies mentioned above reported a decrease in the band gap after modification of the catalyst surface. Wahyuni et al. [85] and Sambaza et al. [75] described a decrease from 3.2 eV to 3.0 eV, due to the incorporation of Ag and SiO₂ on the surface of TiO₂, respectively. Habtamu et al. [72] registered decreases from 3.3 eV to 2.87 eV and to 2.61 eV, after Ag and PANI deposition on ZnO and Ag-ZnO, respectively. Mohammed et al. [52] detected a decrease from 3.3 eV to 2.50 eV and then an increase to 2.68 eV, after Cu₂O deposition on ZnO and the subsequent PANI deposition onto Cu₂O-ZnO. Sharma et al. [71] reported shrinkages to 2.46 eV and to 1.80 eV after FeO deposition on ZnO and the deposition of PANI on FeO-ZnO.

Table 9. Summary of studies that have analyzed the effect of modifying the catalyst surface on the PANI-supported photocatalysis process.

Composite	Immobilization Technique	Conditions Tested	Results	Reference
Ag-TiO ₂ /PANI powder	In situ polymerization	[BPA] ₀ = 5 mg/L T = 25 °C 500 W halogen lamp or 400 W UV lamp t = 55 min for UV and 110 min for visible light irradiation Ag/TiO ₂ = 2 wt.%	BG = 3 eV 99.7% removal k = 0.034 min ⁻¹ for UV k = 0.0285 min ⁻¹ for visible light	[75]
SiO ₂ -TiO ₂ /PANI powder	In situ polymerization	[MB] ₀ = 10 mg/L 9.2 wt.% PANI 100 W xenon lamp t = 90 min	BG = 3 eV 26% removal (k = 0.003 min ⁻¹)	[85]
ZnO-TiO ₂ /PANI powder	In situ polymerization	[P-Cresol] ₀ = 100 ppm 25 W UV lamp t = 6 h	99% removal (k = 0.013 min ⁻¹)	[53]
Ag-ZnO/PANI powder	In situ polymerization	[MG] ₀ = 200 mg/L Visible light pH = 8 t = 120 min	BG = 2.61 eV 98.6% removal (k = 0.036 min ⁻¹)	[72]
Cu ₂ O-ZnO/PANI powder	In situ polymerization	[CR] ₀ = 30 mg/L 100 W LED light Cu ₂ O-ZnO/Aniline = 10 g/mL t = 30 min pH = 6	BG = 2.68 eV 95% removal (k = 0.10 min ⁻¹)	[52]
FeO-ZnO/PANI powder	In situ polymerization	[3-APh] ₀ = 10 mg/L Sunlight t = 120 min	BG = 1.8 eV 92% removal (k = 0.021 min ⁻¹)	[71]

Another way to improve the performance of the PANI composite is by avoiding leaching of the catalyst, namely, ZnO, because it can easily be dissolved by the addition of diethylene glycol (DEG). Both Eskizeybek et al. [76] and Gilja et al. [86] tested the addition of DEG to ZnO/PANI, as summarized in Table 10. Gilja et al. [86] found that the addition of DEG hindered the dissolution of ZnO, which slowly decreased the pH of the polymerization media (PANI conductivity considerably increases during synthesis in acidic media). In addition, with the increase in DEG concentration, the polymer BG decreases (from 2.22 to 2.13 eV), which enables better photocatalytic activity under visible radiation [76,86]. The number of spherical catalyst particles deposited on the support increases with the increase in DEG concentration, and consequently, so does the number of active sites [76,86]. Eskizeybek et al. [76] also found that the presence of DEG enhances the formation of quinoid segments, due to the use of acidic solvents during polymerization.

Improvements in stability are enhanced through the use of commercially available catalyst nanoparticles (NPs). When NPs prepared in the laboratory are used, after 3–5 uses, there is a 15% decrease in pollutant removal [55,87]. If opting for commercially available NPs, after 6 reuses, there is a decrease of 1–8% [49,88].

The analysis of chemical species involved in the photocatalytic degradation of CEC has also been the subject of research. The main contributors to this process have been identified by scavenging tests using benzoquinone (BQ), as a scavenger for O₂^{•-}, isopropanol (IPA) for OH[•] and ethylenediaminetetraacetic acid (EDTA) or ammonium oxalate (AO) as scavengers for holes. Asgari et al. [49] found that OH[•] radicals are key contributors for the degradation of MNZ, at a pH of 7, followed by O₂^{•-} and holes. This result was

expected, because according to Mohammed et al. [52], Ghule et al. [65], and Sambaza et al. [67], at lower pHs, holes are key contributors to the photocatalytic activity, whereas at neutral or high pH, hydroxyl radicals are believed to be the key oxidant moieties. However, Mohammed et al. [52] found that holes are the main contributors for the degradation of CR, at a pH of 6, followed by $O_2^{\bullet-}$ and OH^{\bullet} . Similarly, Sambaza et al. [67] concluded that, at a pH of 10, the degradation of BPA is enhanced in the presence of holes. The reasons are that: (i) attack of the holes is faster than the rate of OH^{\bullet} radical formation; and (ii) the lifetime of OH^{\bullet} radicals is very short, because they decay or are scavenged within a very few angstroms from the site of generation, unlike $O_2^{\bullet-}$ radicals which can diffuse up to tens of micrometers from their generation site, thus exerting a long-range effect.

Table 10. Summary of studies that have analyzed the effect of adding DEG on the PANI-supported photocatalysis process.

Composite	Immobilization Technique	Conditions Tested	Results	Reference
ZnO/PANI powder	In situ polymerization	$[MB]_0 = [MG]_0 = 10^{-5}$ M 15 W UV lamp and solar irradiation $t = 5$ h for solar irradiation and 9 h for UV irradiation [DEG] = 1 M	Solar: 99% removal of both dyes ($k = 0.015 \text{ min}^{-1}$) UV: MB removal of 80% ($k = 0.003 \text{ min}^{-1}$) MG removal of 90% ($k = 0.004 \text{ min}^{-1}$)	[76]
ZnO/PANI powder	In situ polymerization	$[AB25]_0 = 30$ mg/L 17.6 wt.% PANI 450 W solar irradiation simulator pH = 7 $t = 60$ min [DEG] = {0.02, 0.024, 0.04} M	[DEG] = 0.04 M 89% removal ($k = 0.037 \text{ min}^{-1}$)	[86]

3.2. PVA-Supported Photocatalysis

As previously mentioned, PVA can be used as a support due to the bonds that it creates with the catalyst. The OH groups on the surface of nanoparticles react with the OH groups in PVA, forming Ti-O-C bonds [60]. However, this crosslink point does not provide the composite with good stability, due to its solubility, which is enhanced upon increasing the temperature; this could contribute to higher mass reductions in irradiated systems, such as photocatalysis [89]. However, Hegedus et al. [89] discovered that thermally treated PVA exhibits a smaller mass reduction (2%) than untreated PVA (42%).

Under heat treatment, random PVA chains in amorphous regions are rearranged to form an ordered and denser crystalline region [60]. The crystalline regions and the Ti-O-C bonds act as physical and chemical crosslinking points, respectively, to form a three-dimensional network, endowing the hybrid film with excellent mechanical stability and swelling ability in water [60]. Additionally, the swelling ability of crosslinked PVA obtained by chemical or physical crosslinking methods can ensure that the embedded photocatalyst nanoparticles are fully in contact with the pollutants [60]. In addition, (i) Lei et al. [60] and Ghule et al. [65] verified that the treated catalyst/PVA matrix exhibited higher efficiency than the untreated matrix, because the untreated one displayed many catalyst aggregates and a non-homogeneous dispersion; (ii) Yan et al. [47] and Yan et al. [48] found that the heat treatment yields a transparent film; (iii) Yan et al. [47] and Song et al. [79] found that treating the PVA extends the light absorption of TiO_2 to the visible light region, as far as 800 nm; (iv) Yan et al. [47], Wang et al. [54], and Ren et al. [68] reported that heat treatment improves the stability of the materials, which could be reused 5–8 times without efficiency loss. Furthermore, Lei et al. [60] reused the materials for 25 cycles without a loss of efficiency. However, some attention must be given to the treatment temperature, because it controls the crystallinity degree of the material, and can cause PVA degradation, change

its swelling degree, and alter the surface area [47,48,54,60]. The conditions tested in the aforementioned studies and the results are presented in Table 11.

Table 11. Summary of studies that have analyzed the effect of the heat treatment on the PVA-supported photocatalysis process.

Composite	Immobilization Technique	Conditions Tested	Results	Reference
TiO ₂ /PVA film	Mixing	[MO] ₀ = 15 mg/L 60.9 W/m ² UV lamp 10 wt.% TiO ₂ t = 5 h Treatment: heat treated under vacuum at 140–200 °C for 0.5–10 h	Treated at 140 °C for 2 h: ~100% removal (k = 0.015 min ⁻¹)	[60]
TiO ₂ /PVA film	Mixing	[Triton X – 100] ₀ = 2 × 10 ⁻⁴ M 40 wt.% PVA Solar simulator 720 W/m ² t = 6 h Treatment: heated at 140 °C for 2 h under argon	62% removal (k = 0.003 min ⁻¹)	[89]
ZnO/PVA powder	Mixing	[MO] ₀ = 20 mg/L 400 kW/m ² mercury lamp 8 wt.% ZnO t = 80 min Treatment: 10 min under a 695 W microwave radiation; Annealing at 200 °C for 1 h	95% removal (k = 0.05 min ⁻¹)	[65]
TiO ₂ /PVA film	Hydrothermal	[MO] ₀ = 10 mg/L 200 W dysprosium lamp 10 wt.% PVA t = 40 h Treatment: Treated at 140–240 °C	Treated at 180 °C: 84% removal (k = 0.0008 min ⁻¹)	[54]
TiO ₂ /PVA film	Hydrothermal	[Cr(VI)] ₀ = 10 ppm 1 W/m ² xenon lamp or 5 W/m ² UV lamp or 1.05 W/m ² solar irradiation 20 wt.% TiO ₂ t = 25 min Treatment: heated at 150 °C for 3 h in an autoclave	UV and solar: 100% removal (k = 0.18 min ⁻¹) Xenon lamp: 90% removal (k = 0.09 min ⁻¹)	[47]
TiO ₂ /PVA film	Hydrothermal	[MO] ₀ = 15 mg/L 600 W/m ² xenon lamp 40 wt.% TiO ₂ t = 50 min Treatment: heated at 110–150 °C for 1–3 h in an autoclave	Treated at 110 °C for 3 h: 95% removal (k = 0.060 min ⁻¹)	[48]

Table 11. Cont.

Composite	Immobilization Technique	Conditions Tested	Results	Reference
ZnO/PVA film	Sol-gel	[RhB] ₀ = 10 mg/L 700 W/m ² tungsten-halogen lamp 16.7 wt.% PVA t = 6 h Treatment: Treated at 120–240 °C for 4 h in a flow of N ₂ gas	Treated at 180 °C for 4 h: 89% removal (k = 0.006 min ⁻¹) Untreated: 7 % removal (k = 0.0002 min ⁻¹)	[79]

As mentioned above, the heat treatment process makes the material visible-light-responsive. However, the same outcome is achieved through the catalyst doping process. According to Khan et al. [58], the doping of ZnO with Al₂O₃ allows the composite to absorb light with wavelengths (WLs) in the range of 400–800 nm and to reduce its thermal decomposition. However, Jiang et al. [90] found that, before and after doping TiO₂ with Mo, the UV-Vis absorption spectrum of the composite does not change, because its BG remains the same. Sekar et al. [91] found that doping ZnO with iron and thermally treating the composite by calcination induces a decrease in the BG from 3.3 to 3.0 eV. Thus, it can be concluded that the effectiveness of the doping process is dependent on the dopant used and the amount which is introduced. Comparing the results from Montallana and Vasquez Jr. [92] with those from Montallana et al. [13], it is possible to conclude that the doping process with Ag was responsible for turning the material visible-light-responsive. In these experiments, the materials were prepared with the same protocol and the photocatalytic process was performed in the same conditions, the radiation source being the only difference. From these investigations, it can also be concluded that both processes achieved similar reaction kinetics. In Table 12, a summary of these results is presented.

The selected immobilization technique also affects the process efficiency, as shown in Table 13. Analyzing the data in Table 13, which are based on the pseudo-first-order kinetic constants for the pollutants' degradation, it can be concluded that:

- (i) For MO degradation, excluding the effects of radiation, reactor configuration and geometry:
 - When a photocatalyst is immobilized by the hydrothermal method, if the TiO₂:MO ratio is in the order of hundreds, low kinetic constants are achieved. Thus, it is preferable to use ratios in the order of tens;
 - To achieve similar kinetic constants, the immobilization of ZnO by the sol-gel procedure requires a smaller amount of photocatalyst to be introduced into the reaction medium. This configuration is followed by hydrothermal TiO₂ immobilization and TiO₂ immobilization by mixing.
- (ii) For MB degradation, excluding the effects of radiation, configuration, and reactor geometry, ZnO immobilization by the sol-gel procedure, when compared with TiO₂ immobilization by mixing, yields higher kinetics, while using smaller amounts of photocatalyst;
- (iii) For the degradation of RhB, excluding the effects of radiation intensity and reactor geometry, the immobilization of ZnO by the sol-gel procedure yields higher reaction constants compared with the immobilization of TiO₂ by mixing, when the same amount of photocatalyst is introduced into the reaction medium.

Therefore, considering the information available in the literature and discussed above, immobilization of the photocatalyst by the sol-gel process, for the subsequent manufacture of catalyst/PVA materials in the form of films or powders, seems to be the most suitable immobilization technique.

Table 12. Summary of studies that have analyzed the effect of doping the catalyst on the PVA-supported photocatalysis process.

Composite	Immobilization Technique	Conditions Tested	Results	Reference
Al ₂ O ₃ -ZnO/PVA film	Mixing	[MB] ₀ = 5 mg/L Solar radiation t = 30 min	WL = [400, 800] nm 100% removal (k = 0.15 min ⁻¹)	[58]
Fe-ZnO/PVA film	Mixing	[Nph] ₀ = 40 ppm 16 W UV lamp t = 4 h	BG = 3 eV 96% removal (k = 0.013 min ⁻¹)	[91]
Mo-TiO ₂ /PVA film	Sol-gel	[MB] ₀ = 10 ⁻⁵ M 8 W UV lamp t = 24 h 0.2 wt.% Mo	BG = 3.3 eV 91% removal (k = 0.002 min ⁻¹)	[90]
Ag-TiO ₂ /PVA film	Mixing	[MB] ₀ = 3 ppm 33 W/m ² LED lamp t = 6 h	51% removal (k = 0.002 min ⁻¹)	[92]
TiO ₂ /PVA film	Mixing	[MB] ₀ = 2.5 ppm 56 W UV lamp t = 360 min	12 wt.% PVA solution 70% removal (k = 0.003 min ⁻¹)	[13]

Table 13. Immobilization technique effect on the kinetic rate of the PVA-supported photocatalysis process.

Pollutant	Composite	Immobilization Technique	Conditions Tested and Results	Reference					
MO	TiO ₂ /PVA film	Hydrothermal	200 W dysprosium lamp 150 mg _{TiO₂} /g _{MO} → 5.2 × 10 ⁻⁴ min ⁻¹ 200 mg _{TiO₂} /g _{MO} → 6.3 × 10 ⁻⁴ min ⁻¹ 225 mg _{TiO₂} /g _{MO} → 1.0 × 10 ⁻³ min ⁻¹ 237.5 mg _{TiO₂} /g _{MO} → 3.3 × 10 ⁻⁴ min ⁻¹	[54]					
			TiO ₂ /PVA film	Hydrothermal	600 W/m ² xenon lamp 2.22 mg _{TiO₂} /g _{MO} → 1.83 × 10 ⁻² min ⁻¹ 4.44 mg _{TiO₂} /g _{MO} → 3.22 × 10 ⁻² min ⁻¹ 6.66 mg _{TiO₂} /g _{MO} → 4.61 × 10 ⁻² min ⁻¹ 8.88 mg _{TiO₂} /g _{MO} → 5.99 × 10 ⁻² min ⁻¹	[48]			
						TiO ₂ /PVA film	Mixing	6 0.9 W/m ² UV lamp 66.6 mg _{TiO₂} /g _{MO} → 1.50 × 10 ⁻² min ⁻¹	[60]
						ZnO/PVA powder	Mixing	400 kW/m ² mercury lamp 0.8 mg _{TiO₂} /g _{MO} → 5.00 × 10 ⁻² min ⁻¹	[67]
	ZnO/PVA powder	Sol-gel	400 W halogen-mercury lamp 0.0095 mg _{TiO₂} /g _{MO} → 8.87 × 10 ⁻³ min ⁻¹ 0.0093 mg _{TiO₂} /g _{MO} → 1.34 × 10 ⁻² min ⁻¹ 0.0090 mg _{TiO₂} /g _{MO} → 1.81 × 10 ⁻³ min ⁻¹	[56]					
	MB	TiO ₂ /PVA film	Mixing	4 × 10 W UV light 25 mg _{TiO₂} /g _{MO} → 4.0 × 10 ⁻³ min ⁻¹	[93]				
ZnO/PVA powder		Sol-gel	400 W halogen-mercury lamp 0.0095 mg _{TiO₂} /g _{MO} → 8.9 × 10 ⁻³ min ⁻¹ 0.0093 mg _{TiO₂} /g _{MO} → 1.3 × 10 ⁻² min ⁻¹ 0.0090 mg _{TiO₂} /g _{MO} → 1.8 × 10 ⁻³ min ⁻¹	[56]					

Table 13. Cont.

Pollutant	Composite	Immobilization Technique	Conditions Tested and Results	Reference
			18 W LED lamp	
	TiO ₂ /PVA film	Mixing	2 mg _{TiO₂} /g _{MO} → 1.7 × 10 ⁻⁶ min ⁻¹	[59]
			6 mg _{TiO₂} /g _{MO} → 1.7 × 10 ⁻⁶ min ⁻¹	
			10 mg _{TiO₂} /g _{MO} → 4.0 × 10 ⁻⁷ min ⁻¹	
			20 mg _{TiO₂} /g _{MO} → 1.2 × 10 ⁻⁵ min ⁻¹	
			40 mg _{TiO₂} /g _{MO} → 2.2 × 10 ⁻⁵ min ⁻¹	
RhB			700 W/m ² tungsten-halogen Lamp	
	ZnO/PVA film	Sol-gel	20.1 mg _{TiO₂} /g _{MO} → 1.0 × 10 ⁻⁴ min ⁻¹	[79]
			22.5 mg _{TiO₂} /g _{MO} → 6.0 × 10 ⁻⁴ min ⁻¹	
			24.0 mg _{TiO₂} /g _{MO} → 2.5 × 10 ⁻³ min ⁻¹	
			25.0 mg _{TiO₂} /g _{MO} → 6.4 × 10 ⁻³ min ⁻¹	
			25.6 mg _{TiO₂} /g _{MO} → 4.5 × 10 ⁻³ min ⁻¹	
			26.7 mg _{TiO₂} /g _{MO} → 2.5 × 10 ⁻³ min ⁻¹	

3.3. PDMS-Supported Photocatalysis

The use of PDMS in photocatalytic materials was introduced by Iketani et al. [94], where it was applied as an intermediate layer between polymethylmethacrylate (PMMA) substrate and the TiO₂ photocatalyst to slow down the photocorrosion which is caused by PMMA/TiO₂ interactions [95]. In fact, the chemical stability of PDMS, against the corrosive effect of some common photocatalysts (ZnO, TiO₂, and CuO), provided by siloxane chemical bonds, is its main advantage [82,96]. PDMS presents other benefits, such as its sticky surface, which acts as a binder and increases the adhesion of catalyst particles to the substrate; its stability under irradiation; and its flexibility, which makes it suitable for use on curved surfaces [95,96]. However, PDMS is not stable in strongly alkaline environments; it is better suited for solutions with a neutral pH and using ZnO, which is also sensitive to alkaline environments, as the photocatalyst [95].

According to some authors, the inherent hydrophobicity of PDMS is a disadvantage because it does not exert a high affinity of the surface towards H₂O [97]. However, other authors point to the use of hydrophobic composites, due to their self-cleaning and fouling resistance characteristics [98,99]. Wang et al. [61] verified that after 5 cycles, TiO₂/PDMS maintained its performance. Furthermore, Deng et al. [98] concluded that, even after 400 washes, the composite maintained its characteristics. Wang et al. [99] and Santiago et al. [100] found that the hydrophobicity of the composites does not influence its catalytic activity; under UV radiation, the contact angle decreases by up to 90°.

One way to change this characteristic is by thermally treating the PDMS, as reported in Table 14. According to Deng et al. [98] and Wang et al. [61], at temperatures above 400 °C, the surface exhibits hydrophilic properties, due to PDMS degradation and the simultaneous exposure of hydrophilic TiO₂ particles. Park et al. [14] and Jeong et al. [97] denoted that, after the heat treatment, at or above 700 °C, the methyl groups present in PDMS disappear, carbonyl groups are formed, and the composite becomes hydrophilic. According to Gomes et al. [34], the amount of catalyst immobilized in the PDMS surface can also affect the hydrophobicity of the material. In this study, a plasma-treated PDMS membrane was immersed in TiO₂ suspensions with different concentrations to create TiO₂/PDMS membranes. The water contact angles (WCA) of the different membranes were measured, and it was concluded that the presence of TiO₂ lowers the material WCA and increasing the amount of TiO₂ increases the WCA.

To extend the spectral response of the composite to the visible light range, some researchers have doped photocatalysts; the obtained results are summarized in Table 15. Lian et al. [73] evaluated the effect of dopant loading on the process performance, by varying it from 5 wt.% to 20 wt.%. It was concluded that an increase in the dopant load caused a decrease in the thermal stability of the composite; thus, for later tests, the smaller

amount of dopant was selected as the best. It was also concluded that the addition of carbon nanotubes doubled the material efficiency. Park et al. [14] found that doping the catalyst with N enabled the composite to absorb radiation in the visible range, due to nitrogen occupying the substantial sites as well as the presence of oxygen vacancies. Lee et al. [78] verified that the addition of Au extended the absorption spectrum of the composite to the visible range, mainly in wavelengths of 500 to 600 nm. Lee et al. [78] also concluded that the addition of gold accelerated the photocatalytic process by 12.5% under UV light, and improved the process efficiency ninefold. It was also concluded that, under visible or UV radiation, the same removal rate of RhB was obtained when Au-TiO₂/PDMS sponges were applied.

Table 14. Temperature effect on the hydrophobicity/hydrophilicity of PDMS membranes and on the kinetic rate of the PDMS-supported photocatalysis process.

Composite	Immobilization Technique	Conditions Tested	Results	Reference
TiO ₂ /PDMS hydrophilic film	Polymer Deposition	[MB] ₀ = 1 ppm 4 W UV lamp <i>t</i> = 60 min T _{annealing} = {700, 800, 1000} °C	T _{annealing} = 700 °C 70% removal (<i>k</i> = 0.02 min ⁻¹) T _{annealing} = 800 °C 90% removal (<i>k</i> = 0.038 min ⁻¹) T _{annealing} = 1000 °C 20% removal (<i>k</i> = 0.004 min ⁻¹)	[97]
TiO ₂ /PDMS hydrophilic film	Polymer Deposition	MB UV lamp 33 wt.% TiO ₂ <i>t</i> = 10 min T _{deposition} = {180, 200, 250} °C T _{annealing} = 800 °C	T _{deposition} = 180 °C 71% removal (<i>k</i> = 0.123 min ⁻¹)	[101]
TiO ₂ /PDMS hydrophobic film	Polymer Deposition	[ATTO] ₀ = 1 µg/L 26 W/m ² UV lamp <i>t</i> = 2 h T _{annealing} = 500 °C	90% removal (<i>k</i> = 0.02 min ⁻¹)	[42]
TiO ₂ /PDMS super-hydrophobic coating	Mixing	[MB] ₀ = 0.01 m M Solar radiation 75 wt.% TiO ₂ <i>t</i> = 6 d T _{calcination} = 120 °C	~100% removal (<i>k</i> = 0.001 min ⁻¹)	[61]
		Oleic Acid 48 W mercury lamp 75 wt.% TiO ₂ <i>t</i> = 30 min	~100% removal (<i>k</i> = 0.15 min ⁻¹)	
SiO ₂ -TiO ₂ /PDMS super-hydrophobic film	Mixing	MB UV lamp <i>t</i> = 30 min T _{calcination} = {200, 300, 450} °C	T _{calcination} = 200 °C ~100% removal (<i>k</i> = 0.30 min ⁻¹)	[85]
ZnO/PDMS hydrophobic coatings	Mixing	[MB] ₀ = 10 ⁻⁵ M 6 x 42.8 W/m ² UV lamp <i>t</i> = 90 min	25% removal (<i>k</i> = 0.015 min ⁻¹)	[100]
ZnO/PDMS super-hydrophobic film	Polymer Deposition	[MB] ₀ = 12 mg/L 350 W xenon lamp <i>t</i> = 3 h	99% removal (<i>k</i> = 0.026 min ⁻¹)	[99]

Table 14. Cont.

Composite	Immobilization Technique	Conditions Tested	Results	Reference
N-ZnO/PDMS hydrophilic film	Polymer Deposition	[MB] ₀ = 1 ppm Blue LED 33 wt.% PDMS t = 4 h T _{heat treatment} = 800 °C	50% removal (k = 0.003 min ⁻¹)	[14]

Table 15. Catalyst doping effect on the PDMS-supported photocatalysis process.

Composite	Immobilization Technique	Conditions Tested	Results	Reference
C-TiO ₂ /PDMS microfluid	Mixing	[RhB] ₀ = 13 mg/L 500 W UV lamp 2 C-TiO ₂ wt.% pH = 3 t = 3 h C/TiO ₂ = {5, 10, 20} wt.%	C/TiO ₂ = 5 wt.% 86% removal (k = 0.011 min ⁻¹)	[73]
Au-TiO ₂ /PDMS sponge	Sugar Template	[RhB] ₀ = 20 µM 20 mW LED lamp t = 90 min	~90% removal (k = 0.026 min ⁻¹)	[78]
N-TiO ₂ /PDMS film	Polymer Deposition	[MB] ₀ = 1 ppm Blue LED 33 wt.% PDMS t = 4 h	~100% removal (k = 0.019 min ⁻¹)	[14]

3.4. Plastic Waste as Supports

Recently, the immobilization of catalysts in plastic wastes has been studied to reuse a material that otherwise would be deemed a waste. This approach is linked to the concepts of the circular economy and zero waste, because it promotes the reuse of a product for a new purpose. Therefore, several authors have analyzed the application of PET bottles and PET and PS food containers as photocatalyst supports, as shown in Table 13.

In these studies, the heterogeneous photocatalysis process was optimized by studying the effect of operating parameters such as TiO₂ load, pollutant concentration, and pH value. Comparing the effect of operating conditions, when using plastic wastes or synthesized polymers, it is concluded that their influence on both processes is identical. In addition, the radiation source, the number of immersions during dip-coating, the presence of H₂O₂, and the type of polymer used were also evaluated.

Regarding the best radiation source, it was expected that the use of an artificial UV source would be better than the use of natural radiation, considering the BG of TiO₂ and ZnO. In fact, comparing the studies that use solar radiation with those that apply UV radiation, presented in Table 16, it appears that the process under solar radiation takes longer. However, Barbosa et al. [102] found that both sources achieve the same removal after the same time, due to the presence of H₂O₂ which suppresses the recombination of e⁻/h⁺. Additionally, among the variables studied in the UV/H₂O₂/TiO₂ system, the most influential on the efficiency of the degradation process was the hydrogen peroxide concentration.

Table 16. Summary of the studies that have applied plastic wastes as supports in polymer-supported photocatalysis.

Support	Pollutant	Catalyst	Conditions Tested	Results	Reference
	Paracetamol	TiO ₂	[Paracetamol] ₀ = 2 mg/L 8 W UV lamp 0.1 mg TiO ₂ /cm ² t = 75 min	86% removal (k = 0.027 min ⁻¹)	[83]
	<i>E. coli</i>	TiO ₂	[<i>E. coli</i>] ₀ = 1000 cell/mL 40 W/m ² UV lamp t = 90 min	100% removal	[103]
	4-CP and 2,4-D	TiO ₂	[4-CP] ₀ = 0.2 mM [2,4-D] ₀ = 0.5 mM 0.1 g TiO ₂ /m ² 5.9 W/m ² solar radiation t = 18 h for 4-CP and 12 h for 2,4-D	4-CP removal of 77% (k = 0.0013 min ⁻¹) 2,4-D removal of 65% (k = 0.0014 min ⁻¹)	[104]
PET	As	TiO ₂	[As(III)] ₀ = 1 mg/L 7 mg/L Fe(II) 12 kW/m ² Solar Radiation pH = 7 t = 120 min	99% removal (k = 0.038 min ⁻¹)	[105]
	PR	TiO ₂	[PR] ₀ = 100 mg/L 128 W/m ² solar radiation t = 12 h	98% removal (k = 0.005 min ⁻¹)	[106]
	<i>E. coli</i>	ZnO	[<i>E. coli</i>] ₀ = 3 × 10 ⁸ CFU 30 W/m ² UV lamp t = 90 min	100% removal	[107]
	RB and YT	TiO ₂	[RB] ₀ = [YT] ₀ = 35 mg/L 8.3 W/m ² UV lamp or 16.4 W/m ² Solar Radiation [H ₂ O ₂] = 5.79 mM t = 240 min	UV: 98.2% removal (k = 0.017 min ⁻¹) Solar: 85.5% removal (k = 0.008 min ⁻¹)	[102]
PS	AB83 and DM1	TiO ₂	[AB83] ₀ = [DM1] ₀ = 50 ppm 8 W UV lamp pH = 2.5 t = 30 min	AB83 removal of 93.7% (k = 0.092 min ⁻¹) DM1 removal of 91.9% (k = 0.085 min ⁻¹)	[108]
	AB83 and DM1	ZnO	[AB83] ₀ = [DM1] ₀ = 50 ppm 8 W UV lamp t = 50 min	AB83 removal of 92.1% (k = 0.051 min ⁻¹) DM1 removal of 92.9% (k = 0.053 min ⁻¹)	

The number of immersions affects the amount of TiO₂ immobilized. This is expected to enhance the photocatalytic activity of the films by providing greater surface area availability for the oxidation reactions to take place. However, De Barros et al. [83] concluded that the surface available on which the substrate could react improved by increasing the deposition of TiO₂ for up to five immobilization steps, when the kinetic constant reached its highest value. When greater amounts of TiO₂ were deposited, the kinetic constant remained approximately the same, probably because the PET surface was completely covered after five immobilization steps. Sandoval et al. [108] proved that the optimum number of immobilizations steps is dependent on the particle size. In this study, more immersions were necessary to achieve a complete coverage, because the photocatalyst particles used had a smaller diameter than those applied by De Barros et al. [83].

Sandoval et al. [108] compared the immobilization of TiO₂ and ZnO on PET or PS food containers, and verified that both photocatalysts adhere better on PS, because a higher amount of photocatalyst is presented on this material. However, on PS, ZnO is present in the form of agglomerates and the increase in the TiO₂-immobilized mass on PS compared with that in PET is only 5%. The influence of this increase in the reaction constant is uncertain, because on some occasions it did not show any influence, and on others it induced an increase or decrease in the reaction speed.

Few studies have analyzed the reuse of TiO₂/PET bottles; however, those which have concluded that there is no significant decrease in pollutant removal after six cycles [102,103].

4. Process Limitations and Future Perspectives

In this review the effectiveness of the polymer-supported process is recognized, despite its limitations. Photocatalytic oxidation using such materials is a viable alternative to other AOPs, such as (i) Fenton, because it is efficient in a larger pH range and not responsible for the production of residues [6,7]; and (ii) heterogeneous suspended photocatalysis, because it eliminates the catalyst separation step, making the process more economically viable [10,11]. Comparing the photocatalysis process with suspended particles and supported catalysts, there are still other advantages that must be highlighted. The use of polymeric supports reduces the probability of recombination between the photogenerated pairs, thus achieving higher efficiencies [49]. The visible spectrum of solar radiation can be used, without needing to dope the catalyst (depending on the selected polymer and/or its treatment) [49,58]. Moreover, the catalyst can be immobilized into the polymeric matrix, therefore protecting it from carryover during the washing process [9].

Despite its effectiveness, this process also presents some limitations worth mentioning. These limitations can be divided in two main groups: limitations linked to the polymer, and limitations associated with the material form. Regarding the first group of limitations, this includes restrictions associated to the characteristics of the polymer, such as its solubility, hydrophobicity, photodegradation, etc. Polymers such as PVA exhibit high solubility in water; therefore, using it as a support decreases the reusability of the material [89]. Fortunately, its solubility can be minimized by thermally treating the material. This process, however, decreases the transparency and the swelling ability of the material, depending on the temperature and processing time selected [47,48,54,60]. Other polymers, such as PDMS, are inherently hydrophobic; therefore, water does not wet its surface. Fortunately, this characteristic can be altered under radiation, through thermal treatment or by surface modification processes [14,34,61,97,98]. Another disadvantage of polymers is the possibility of them being photodegraded by the catalysts they support, specifically if they are organic polymers [82]. The material form (film, particle, or sponge) can also limit the process efficiency because, for example, the use of particles can cause effluent turbidity and reduce the material's ability to absorb light. It can also affect the process simplicity, because materials such as sponges and films have simpler and easier cleaning processes [70,72]. To overcome these limitations, different treatment process must be analyzed, investigated, optimized, and compared, such as thermal treatment or surface modification processes. The applicability of different polymers in similar photocatalytic processes should also be taken in consideration, to evaluate which one presents the best performance, which requires the least catalyst, which has the simplest preparation protocol, etc.

Despite the advances achieved and the relevance of the studies mentioned throughout this review, there are still gaps to be filled in the scientific knowledge of the applicability of these materials in the process in question, namely:

- (i) Few studies have explored optimization of the process, regarding the characteristics of the material and the operating conditions, which is a complex subject because the optimal material composition is dependent on the polymer used, the immobilization technique applied, and the pollutant to be remove. However, regarding the radiation source and the pH value, it is of interest to investigate the effectiveness of the

- process under solar radiation and using the inherent pH of the effluent to minimize operating costs;
- (ii) To the best of our knowledge, no study has assessed the importance of the influence of variables on the process objective, to verify which should be controlled more strictly;
 - (iii) As far as we are aware, no study has evaluated the influence that the immobilization technique has on the characteristics of the material and/or the degradation of the pollutant, and there is little information in the literature that allows this analysis to be carried out;
 - (iv) To the best of our knowledge, studies that apply waste plastics as supports have only investigated dip-coating as an immobilization technique. Furthermore, PET bottles are usually utilized as reactors, which limits the scale-up ability;
 - (v) Most studies have focused on the applicability of this process in the treatment of colored effluents, which become an obstacle to its efficiency, as they affect the capacity of the catalyst to absorb radiation;
 - (vi) Few studies have evaluated the effect of adding other oxidizing agents (such as hydrogen peroxide) to the reaction medium, to promote an acceleration in the photocatalytic process;
 - (vii) To the best of our knowledge, no study has evaluated the performance of the process in terms of the toxicity of the treated effluent;
 - (viii) There are lacks in the literature regarding the applications of these materials in the photocatalytic oxidation of real wastewater, or complex mixtures. This is crucial to understand the material's behavior under real water treatment conditions;
 - (ix) The operation of these supported catalysts in continuous operation reactors at bench and pilot scale must be considered to elucidate their activity and stability during long-term operation;
 - (x) Configuring the reactors to optimize the process using supported catalysts, bearing in mind mass transfer limitations as well as light penetration, should be considered.

The questions raised above are relevant, because their answers would develop understanding of the process and enable us to move forward in the sense of making the process a closer reality. Thus, future investigations should focus on these questions.

5. Conclusions

Through the critical literature analysis, it is possible to conclude that special attention must be given to the operation conditions and the conditions applied during the preparation of the materials, because these influence the physicochemical characteristics of the composites, and consequently, the efficiency of the process. It was also verified that the studied materials are effective in degrading the analyzed pollutants, under optimal conditions. However, it is not possible to conclude which is the best material, because in certain cases they have not been applied for the degradation of the same pollutants, nor under the same radiation. Furthermore, it was not possible to find a viable variable that could be used as the common independent variable. In this review, it has also been verified that polymer-supported photocatalysis is able to achieve excellent removal efficiency, in the treatment of synthetic wastewater; however, there are still relevant questions to be answered before the realization of this process.

Author Contributions: Writing—original draft preparation, M.J.S.; Conceptualization, M.J.S., J.G., P.F. and R.C.M.; Formal analysis, M.J.S., J.G., P.F. and R.C.M.; Writing—review and editing, J.G., P.F. and R.C.M.; Supervision, J.G., P.F. and R.C.M.; Funding acquisition, J.G., P.F. and R.C.M. All authors have read and agreed to the published version of the manuscript.

Funding: This work was financed by European Structural and Investment Funds through Portugal2020 by the project PhotoSupCatal—Development of supported catalytic systems for wastewater treatment by photo-assisted processes (POCI-01-0247-FEDER-047545).

Institutional Review Board Statement: Not applicable.

Informed Consent Statement: Not applicable.

Data Availability Statement: Not applicable.

Acknowledgments: J.G. gratefully acknowledges the Foundation for Science and Technology—FCT (Portugal) for financial support (CEECIND/01207/2018). The researchers from CIEPQPF were supported by Foundation Science and Technology—FCT (Portugal) UIDB/00102/2020.

Conflicts of Interest: The authors declare no conflict of interest.

References

1. Bolong, N.; Ismail, A.F.; Salim, M.R.; Matsuura, T. A review of the effects of emerging contaminants in wastewater and options for their removal. *Desalination* **2009**, *239*, 229–246. [[CrossRef](#)]
2. Ismail, W.N.W.; Mokhtar, S.U. Various Methods for Removal, Treatment, and Detection of Emerging Water Contaminants. In *Emerging Contaminants*; Nuro, A., Ed.; InterOpen: London, UK, 2021; ISBN 978-1-83962-419-3.
3. Rathi, B.S.; Kumar, P.S.; Show, P.-L. A review on effective removal of emerging contaminants from aquatic systems: Current trends and scope for further research. *J. Hazard. Mater.* **2021**, *409*, 124413. [[CrossRef](#)] [[PubMed](#)]
4. Dhangar, K.; Kumar, M. Tricks and tracks in removal of emerging contaminants from the wastewater through hybrid treatment systems: A review. *Sci. Total Environ.* **2020**, *738*, 140320. [[CrossRef](#)] [[PubMed](#)]
5. Rivera-Utrilla, J.; Sánchez-Polo, M.; Ferro-García, M.Á.; Prados-Joya, G.; Ocampo-Pérez, R. Pharmaceuticals as emerging contaminants and their removal from water. A review. *Chemosphere* **2013**, *93*, 1268–1287. [[CrossRef](#)]
6. Gmurek, M.; Gomes, J.; Martins, R.C.; Quinta-Ferreira, R.M. Comparison of radical-driven technologies applied for paraben mixture degradation: Mechanism, biodegradability, toxicity and cost assessment. *Environ. Sci. Pollut. Res.* **2019**, *26*, 37174–37192. [[CrossRef](#)]
7. Oturan, M.A.; Aaron, J.-J. Advanced Oxidation Processes in Water/Wastewater Treatment: Principles and Applications. A Review. *Crit. Rev. Environ. Sci. Technol.* **2014**, *44*, 2577–2641. [[CrossRef](#)]
8. Summerfelt, S.T. Ozonation and UV irradiation—An introduction and examples of current applications. *Aquac. Eng.* **2003**, *28*, 21–36. [[CrossRef](#)]
9. Zakria, H.S.; Othman, M.H.D.; Kamaludin, R.; Kadir, S.H.S.A.; Kurniawan, T.A.; Jilani, A. Immobilization techniques of a photocatalyst into and onto a polymer membrane for photocatalytic activity. *RSC Adv.* **2021**, *11*, 6985–7014. [[CrossRef](#)]
10. Singh, S.; Mahalingam, H.; Singh, P.K. Polymer-supported titanium dioxide photocatalysts for environmental remediation: A review. *Appl. Catal. A Gen.* **2013**, *462–463*, 178–195. [[CrossRef](#)]
11. Bagheri, S.; Julkapli, N.M.; Hamid, S.B.A. Titanium Dioxide as a Catalyst Support in Heterogeneous Catalysis. *Sci. World J.* **2014**, *2014*, 727496. [[CrossRef](#)]
12. Reddy, K.R.; Jyothi, M.S.; Raghu, A.V.; Sadhu, V.; Naveen, S.; Aminabhavi, T.M. Nanocarbons-Supported and Polymers-Supported Titanium Dioxide Nanostructures as Efficient Photocatalysts for Remediation of Contaminated Wastewater and Hydrogen Production. In *Environmental Chemistry for a Sustainable World—Nanophotocatalysis and Environmental Applications*; Inamuddin, Asiri, A.M., Lichtfouse, E., Eds.; Springer: New York, NY, USA, 2020; Volume 30, pp. 139–169. ISBN 978-3-030-12619-3.
13. Montallana, A.D.S.; Lai, B.-Z.; Chu, J.P.; Vasquez, M.R., Jr. Enhancement of photodegradation efficiency of PVA/TiO₂ nanofiber composites via plasma treatment. *Mater. Today Commun.* **2020**, *24*, 101183. [[CrossRef](#)]
14. Park, E.J.; Jeong, B.; Jeong, M.-G.; Kim, Y.D. Synergetic effects of hydrophilic surface modification and N-doping for visible light response on photocatalytic activity of TiO₂. *Curr. Appl. Phys.* **2014**, *14*, 300–305. [[CrossRef](#)]
15. Tran, V.V.; Nu, T.T.V.; Jung, H.-R.; Chang, M. Advanced Photocatalysts Based on Conducting Polymer/Metal Oxide Composites for Environmental Applications. *Polymers* **2021**, *13*, 3031. [[CrossRef](#)] [[PubMed](#)]
16. Teoh, W.Y.; Scott, J.A.; Amal, R. Progress in Heterogeneous Photocatalysis: From Classical Radical Chemistry to Engineering Nanomaterials and Solar Reactors. *J. Phys. Chem. Lett.* **2012**, *3*, 629–639. [[CrossRef](#)] [[PubMed](#)]
17. Ibhaddon, A.O.; Fitzpatrick, P. Heterogeneous Photocatalysis: Recent Advances and Applications. *Catalysts* **2013**, *3*, 189–218. [[CrossRef](#)]
18. Riaz, U.; Ashraf, S.; Kashyap, J. Enhancement of photocatalytic properties of transitional metal oxides using conducting polymers: A mini review. *Mater. Res. Bull.* **2015**, *71*, 75–90. [[CrossRef](#)]
19. Hitam, C.; Jalil, A. A review on exploration of Fe₂O₃ photocatalyst towards degradation of dyes and organic contaminants. *J. Environ. Manag.* **2020**, *258*, 110050. [[CrossRef](#)]
20. Mishra, M.; Chun, D.M. α -Fe₂O₃ as a photocatalytic material: A review. *Appl. Catal. A Gen.* **2015**, *498*, 126–141. [[CrossRef](#)]
21. Shahroodin, N.S.M.; Jaaafar, J.; Rahmat, A.R.; Yusof, N.; Othman, M.H.D.; Rahman, M.A. Superparamagnetic Iron Oxide as Photocatalyst and Adsorbent in Wastewater Treatment—A Review. *Micro Nanosyst.* **2020**, *12*, 4–22. [[CrossRef](#)]
22. Can, F.; Courtois, X.; Duprez, D. Tungsten-Based Catalysts for Environmental Applications. *Catalysts* **2021**, *11*, 703. [[CrossRef](#)]
23. Diehl, R.; Brandt, G.; Saije, E. The crystal structure of triclinic WO₃. *Acta Crystallogr. Sect. B Struct. Crystallogr. Cryst. Chem.* **1978**, *34*, 1105–1111. [[CrossRef](#)]
24. Szilágyi, I.M.; Fórizs, B.; Rosseler, O.; Szegedi, Á.; Németh, P.; Király, P.; Tárkányi, G.; Vajna, B.; Varga-Josepovits, K.; László, K.; et al. WO₃ photocatalysts: Influence of structure and composition. *J. Catal.* **2012**, *294*, 119–127. [[CrossRef](#)]

25. Dai, W.-L.; Ding, J.; Zhu, Q.; Gao, R.; Yang, X. Tungsten containing materials as heterogeneous catalysts for green catalytic oxidation process. In *Catalysis*; Spivey, J.J., Han, Y.F., Dooley, K.M., Eds.; Royal Society of Chemistry: London, UK, 2016; Volume 28, pp. 1–27. ISBN 979-1-78262-427-1.
26. Lu, Y.; Zhang, J.; Wang, F.; Chen, X.; Feng, Z.; Li, C. K₂SO₄-Assisted Hexagonal/Monoclinic WO₃ Phase Junction for Efficient Photocatalytic Degradation of RhB. *ACS Appl. Energy Mater.* **2018**, *1*, 2067–2077. [[CrossRef](#)]
27. Fan, Y.; Liu, Y.; Cui, H.; Wang, W.; Shang, Q.; Shi, X.; Cui, G.; Tang, B. Photocatalytic Overall Water Splitting by SrTiO₃ with Surface Oxygen Vacancies. *Nanomaterials* **2020**, *10*, 2572. [[CrossRef](#)] [[PubMed](#)]
28. Rahman, Q.I.; Ahmad, M.; Misra, S.K.; Lohani, M. Efficient Degradation of Methylene Blue Dye Over Highly Reactive Cu Doped Strontium Titanate (SrTiO₃) Nanoparticles Photocatalyst Under Visible Light. *J. Nanosci. Nanotechnol.* **2012**, *12*, 7181–7186. [[CrossRef](#)]
29. Zhao, W.; Zhao, W.; Zhu, G.; Lin, T.; Xu, F.; Huang, F. Black strontium titanate nanocrystals of enhanced solar absorption for photocatalysis. *CrystEngComm* **2015**, *17*, 7528–7534. [[CrossRef](#)]
30. Alhaji, M.H.; Sanaullah, K.; Khan, A.; Hamza, A.; Muhammad, A.; Ishola, M.S.; Rigit, A.; Bhawani, S.A. Recent developments in immobilizing titanium dioxide on supports for degradation of organic pollutants in wastewater: A review. *Int. J. Environ. Sci. Technol.* **2017**, *14*, 2039–2052. [[CrossRef](#)]
31. Bouarioua, A.; Zerdaoui, M. Photocatalytic activities of TiO₂ layers immobilized on glass substrates by dip-coating technique toward the decolorization of methyl orange as a model organic pollutant. *J. Environ. Chem. Eng.* **2017**, *5*, 1565–1574. [[CrossRef](#)]
32. Hegemann, D.; Brunner, H.; Oehr, C. Plasma treatment of polymers for surface and adhesion improvement. *Nucl. Instrum. Methods Phys. Res. Sect. B Beam Interact. Mater. At.* **2003**, *208*, 281–286. [[CrossRef](#)]
33. Carrino, L.; Moroni, G.; Polini, W. Cold plasma treatment of polypropylene surface: A study on wettability and adhesion. *J. Mater. Process. Technol.* **2002**, *121*, 373–382. [[CrossRef](#)]
34. Gomes, J.; Maniezo, B.; Alves, P.; Ferreira, P.; Martins, R.C. Immobilization of TiO₂ onto a polymeric support for photocatalytic oxidation of a paraben's mixture. *J. Water Process Eng.* **2021**, *2021*, 102458. [[CrossRef](#)]
35. Nemani, S.K.; Annavarapu, R.K.; Mohammadian, B.; Raiyan, A.; Heil, J.; Haque, A.; Abdelaal, A.; Sojoudi, H. Surface Modification of Polymers: Methods and Applications. *Adv. Mater. Interfaces* **2018**, *5*, 1801247. [[CrossRef](#)]
36. Szabová, R.; Černáková, L.; Wolfová, M.; Černák, M. Coating of TiO₂ nanoparticles on the plasma activated polypropylene fibers. *Acta Chim. Slovaca* **2009**, *2*, 70–76.
37. Puma, G.L.; Bono, A.; Krishnaiah, D.; Collin, J.G. Preparation of titanium dioxide photocatalyst loaded onto activated carbon support using chemical vapor deposition: A review paper. *J. Hazard. Mater.* **2008**, *157*, 209–219. [[CrossRef](#)] [[PubMed](#)]
38. Mahlambi, M.M.; Ngila, C.J.; Mamba, B. Recent Developments in Environmental Photocatalytic Degradation of Organic Pollutants: The Case of Titanium Dioxide Nanoparticles—A Review. *J. Nanomater.* **2015**, *2015*, 790173. [[CrossRef](#)]
39. De Filipo, G.; Pantuso, E.; Armentano, K.; Formoso, P.; Di Profio, G.; Poerio, T.; Fontananova, E.; Meringolo, C.; Mashin, A.I.; Nicoletta, F.P. Chemical Vapor Deposition of Photocatalyst Nanoparticles on PVDF Membranes for Advanced Oxidation Processes. *Membranes* **2018**, *8*, 35. [[CrossRef](#)]
40. Wood, D.; Shaw, S.; Cawte, T.; Shanen, E.; Van Heyst, B. An overview of photocatalyst immobilization methods for air pollution remediation. *Chem. Eng. J.* **2020**, *391*, 123490. [[CrossRef](#)]
41. Wooh, S.; Encinas, N.; Vollmer, D.; Butt, H.-J. Stable Hydrophobic Metal-Oxide Photocatalysts via Grafting Polydimethylsiloxane Brush. *Adv. Mater.* **2017**, *29*, 1604637. [[CrossRef](#)]
42. Liu, J.; Ye, L.; Wooh, S.; Kappl, M.; Steffen, W.; Butt, H.-J. Optimizing Hydrophobicity and Photocatalytic Activity of PDMS-Coated Titanium Dioxide. *ACS Appl. Mater. Interfaces* **2019**, *11*, 27422–27425. [[CrossRef](#)]
43. Oliveira, M.; Machado, A.V. Preparation of Polymer-Based Nanocomposites by Different Routes. In *Nanocomposites: Synthesis, Characterization and Applications*; Wang, X., Ed.; Nova Publishers: Hauppauge, NY, USA, 2013; pp. 73–94. ISBN 978-1-62948-226-2.
44. Adnan, M.M.; Dalod, A.R.M.; Balci, M.H.; Glaum, J.; Einarsrud, M.-A. In Situ Synthesis of Hybrid Inorganic–Polymer Nanocomposites. *Polymers* **2018**, *10*, 1129. [[CrossRef](#)]
45. Jangid, N.K.; Jadoun, S.; Yadav, A.; Srivastava, M.; Kaur, N. Polyaniline-TiO₂-based photocatalysts for dyes degradation. *Polym. Bull.* **2021**, *78*, 4743–4777. [[CrossRef](#)]
46. Guo, Q.; Ghadiri, R.; Weigel, T.; Aumann, A.; Gurevich, E.L.; Esen, C.; Medenbach, O.; Cheng, W.; Chichkov, B.N.; Ostendorf, A. Comparison of in Situ and ex Situ Methods for Synthesis of Two-Photon Polymerization Polymer Nanocomposites. *Polymers* **2014**, *6*, 2037–2050. [[CrossRef](#)]
47. Yan, W.; Chen, Q.; Meng, X.; Wang, B. Multicycle photocatalytic reduction of Cr(VI) over transparent PVA/TiO₂ nanocomposite films under visible light. *Sci. China Mater.* **2017**, *60*, 449–460. [[CrossRef](#)]
48. Yan, W.; Chen, Q.; Du, M.; Yang, K.M.; Cai, X.; Meng, X.; Wang, L. Highly Transparent Poly(vinyl alcohol)(PVA)/TiO₂ Nanocomposite Films with Remarkable Photocatalytic Performance and Recyclability. *J. Nanosci. Nanotechnol.* **2018**, *18*, 5660–5667. [[CrossRef](#)]
49. Asgari, E.; Esrafil, A.; Jafari, A.J.; Kalantary, R.R.; Nourmoradi, H.; Farzadkia, M. The comparison of ZnO/polyaniline nanocomposite under UV and visible radiations for decomposition of metronidazole: Degradation rate, mechanism and mineralization. *Process Saf. Environ. Prot.* **2019**, *128*, 65–76. [[CrossRef](#)]
50. Lee, Y.-J.; Lee, H.S.; Lee, C.-G.; Park, S.-J.; Lee, J.; Jung, S.; Shin, G.-A. Application of PANI/TiO₂ Composite for Photocatalytic Degradation of Contaminants from Aqueous Solution. *Appl. Sci.* **2020**, *10*, 6710. [[CrossRef](#)]

51. Zhao, H.; Li, Z.; Lu, X.; Chen, W.; Cui, Y.; Tang, B.; Wang, J.; Wang, X. Fabrication of PANI@TiO₂ nanocomposite and its sunlight-driven photocatalytic effect on cotton fabrics. *J. Text. Inst.* **2021**, *112*, 1850–1858. [[CrossRef](#)]
52. Mohammed, A.M.; Mohtar, S.S.; Aziz, F.; Aziz, M.; Ul-Hamid, A. Cu₂O/ZnO-PANI ternary nanocomposite as an efficient photocatalyst for the photodegradation of Congo Red dye. *J. Environ. Chem. Eng.* **2021**, *9*, 105065. [[CrossRef](#)]
53. Brooms, T.J.; Otieno, B.; Onyango, M.S.; Ochieng, A. Photocatalytic degradation of P-Cresol using TiO₂/ZnO hybrid surface capped with polyaniline. *J. Environ. Sci. Health Part A* **2018**, *53*, 99–107. [[CrossRef](#)]
54. Wang, Y.; Zhong, M.; Chen, F.; Yang, J. Visible light photocatalytic activity of TiO₂/D-PVA for MO degradation. *Appl. Catal. B Environ.* **2009**, *90*, 249–254. [[CrossRef](#)]
55. Saravanan, R.; Sacari, E.; Gracia, F.; Khan, M.M.; Mosquera, E.; Gupta, V.K. Conducting PANI stimulated ZnO system for visible light photocatalytic degradation of coloured dyes. *J. Mol. Liq.* **2016**, *221*, 1029–1033. [[CrossRef](#)]
56. El-Dafrawy, S.M.; Tarek, M.; Samra, S.; Hassan, S.M. Synthesis, photocatalytic and antidiabetic properties of ZnO/PVA nanoparticles. *Sci. Rep.* **2021**, *11*, 11404. [[CrossRef](#)] [[PubMed](#)]
57. Sahu, K.; Rahamn, K.H.; Kar, A.K. Synergic effect of polyaniline and ZnO to enhance the photocatalytic activity of their nanocomposite. *Mater. Res. Express* **2019**, *6*, 095304. [[CrossRef](#)]
58. Khan, M.M.R.; Akter, M.; Amin, K.; Younus, M.; Chakraborty, N. Synthesis, Luminescence and Thermal Properties of PVA–ZnO–Al₂O₃ Composite Films: Towards Fabrication of Sunlight-Induced Catalyst for Organic Dye Removal. *J. Polym. Environ.* **2018**, *26*, 3371–3381. [[CrossRef](#)]
59. Lou, L.; Kendall, R.J.; Ramkumar, S. Comparison of hydrophilic PVA/TiO₂ and hydrophobic PVDF/TiO₂ microfiber webs on the dye pollutant photo-catalyzation. *J. Environ. Chem. Eng.* **2020**, *8*, 103914. [[CrossRef](#)]
60. Lei, P.; Wang, F.; Gao, X.; Ding, Y.; Zhang, S.; Zhao, J.; Liu, S.; Yang, M. Immobilization of TiO₂ nanoparticles in polymeric substrates by chemical bonding for multi-cycle photodegradation of organic pollutants. *J. Hazard. Mater.* **2012**, *227–228*, 185–194. [[CrossRef](#)]
61. Wang, Y.; Huang, Z.; Gurney, R.S.; Liu, D. Superhydrophobic and photocatalytic PDMS/TiO₂ coatings with environmental stability and multifunctionality. *Colloids Surfaces A Physicochem. Eng. Asp.* **2019**, *561*, 101–108. [[CrossRef](#)]
62. Hossain, S.; Chun, D.-M. ZnO decorated polydimethylsiloxane sponges as photocatalysts for effective removal of methylene blue dye. *Mater. Chem. Phys.* **2020**, *255*, 123589. [[CrossRef](#)]
63. Hickman, R.; Walker, E.; Chowdhury, S. TiO₂-PDMS composite sponge for adsorption and solar mediated photodegradation of dye pollutants. *J. Water Process Eng.* **2018**, *24*, 74–82. [[CrossRef](#)]
64. Vijayalakshmi, S.; Kumar, E.; Ganeshbabu, M.; Venkatesh, P.S.; Rathnakumar, K. Structural, electrical, and photocatalytic investigations of PANI/ZnO nanocomposites. *Ionics* **2021**, *27*, 2967–2977. [[CrossRef](#)]
65. Ghule, L.; Patil, A.; Sapnar, K.; Dhole, S.; Garadkar, K. Photocatalytic degradation of methyl orange using ZnO nanorods. *Toxicol. Environ. Chem.* **2011**, *93*, 623–634. [[CrossRef](#)]
66. Chen, C.; Zhao, D.; Zhou, Q.; Wu, Y.; Zhou, X.; Wang, H. Facile Preparation and Characterization of Polyaniline and CeO₂ Co-Decorated TiO₂ Nanotube Array and its Highly Efficient Photoelectrocatalytic Activity. *Nanoscale Res. Lett.* **2019**, *14*, 60. [[CrossRef](#)] [[PubMed](#)]
67. Sambaza, S.S.; Maity, A.; Pillay, K. Polyaniline-Coated TiO₂ Nanorods for Photocatalytic Degradation of Bisphenol A in Water. *ACS Omega* **2020**, *5*, 29642–29656. [[CrossRef](#)] [[PubMed](#)]
68. Ren, M.; Frimmel, F.H.; Abbt-Braun, G. Multi-cycle photocatalytic degradation of bezafibrate by a cast polyvinyl alcohol/titanium dioxide (PVA/TiO₂) hybrid film. *J. Mol. Catal. A Chem.* **2015**, *400*, 42–48. [[CrossRef](#)]
69. Azeez, F.; Al-Hetlani, E.; Arafa, M.; Abdelmonem, Y.; Nazeer, A.A.; Amin, M.O.; Madkour, M. The effect of surface charge on photocatalytic degradation of methylene blue dye using chargeable titania nanoparticles. *Sci. Rep.* **2018**, *8*, 7104. [[CrossRef](#)]
70. Olad, A.; Nosrati, R. Preparation, characterization, and photocatalytic activity of polyaniline/ZnO nanocomposite. *Res. Chem. Intermed.* **2012**, *38*, 323–336. [[CrossRef](#)]
71. Sharma, S.; Sharma, G.; Kumar, A.; Naushad, M.; Mola, G.T.; Kumar, A.; Al-Misned, F.A.; El-Serehy, H.A.; Stadler, F.J. Visibly Active FeO/ZnO@PANI Magnetic Nano-photocatalyst for the Degradation of 3-Aminophenol. *Top. Catal.* **2020**, *63*, 1302–1313. [[CrossRef](#)]
72. Habtamu, F.; Berhanu, S.; Mender, T. Polyaniline Supported Ag-Doped ZnO Nanocomposite: Synthesis, Characterization, and Kinetics Study for Photocatalytic Degradation of Malachite Green. *J. Chem.* **2021**, *2021*, 2451836. [[CrossRef](#)]
73. Lian, Z.; Wei, C.; Gao, B.; Yang, X.; Chan, Y.; Wang, J.; Chen, G.Z.; Koh, K.S.; Shi, Y.; Yan, Y.; et al. Synergetic treatment of dye contaminated wastewater using microparticles functionalized with carbon nanotubes/titanium dioxide nanocomposites. *RSC Adv.* **2020**, *10*, 9210–9225. [[CrossRef](#)]
74. Samadi, M.; Shivaee, H.A.; Zanetti, M.; Pourjavadi, A.; Moshfegh, A. Visible light photocatalytic activity of novel MWCNT-doped ZnO electrospun nanofibers. *J. Mol. Catal. A Chem.* **2012**, *359*, 42–48. [[CrossRef](#)]
75. Sambaza, S.; Maity, A.; Pillay, K. Enhanced degradation of BPA in water by PANI supported Ag/TiO₂ nanocomposite under UV and visible light. *J. Environ. Chem. Eng.* **2019**, *7*, 102880. [[CrossRef](#)]
76. Eskizeybek, V.; Sari, F.; Gülce, H.; Gülce, A.; Avcı, A. Preparation of the new polyaniline/ZnO nanocomposite and its photocatalytic activity for degradation of methylene blue and malachite green dyes under UV and natural sun lights irradiations. *Appl. Catal. B Environ.* **2012**, *119–120*, 197–206. [[CrossRef](#)]

77. Sosnin, I.; Vlassov, S.; Akimov, E.G.; Agenkov, V.I.; Dorogin, L.M. Transparent ZnO-coated polydimethylsiloxane-based material for photocatalytic purification applications. *J. Coat. Technol. Res.* **2020**, *17*, 573–579. [[CrossRef](#)]
78. Lee, S.Y.; Kang, D.; Jeong, S.; Do, H.T.; Kim, J.H. Photocatalytic Degradation of Rhodamine B Dye by TiO₂ and Gold Nanoparticles Supported on a Floating Porous Polydimethylsiloxane Sponge under Ultraviolet and Visible Light Irradiation. *ACS Omega* **2020**, *5*, 4233–4241. [[CrossRef](#)] [[PubMed](#)]
79. Song, Y.; Zhang, J.; Yang, H.; Xu, S.; Jiang, L.; Dan, Y. Preparation and visible light-induced photo-catalytic activity of H-PVA/TiO₂ composite loaded on glass via sol–gel method. *Appl. Surf. Sci.* **2014**, *292*, 978–985. [[CrossRef](#)]
80. Yang, H.; Zhang, J.; Song, Y.; Xu, S.; Jiang, L.; Dan, Y. Visible light photo-catalytic activity of C-PVA/TiO₂ composites for degrading rhodamine B. *Appl. Surf. Sci.* **2015**, *324*, 645–651. [[CrossRef](#)]
81. Tennakone, K.; Tilakaratne, C.; Kottegoda, I. Photocatalytic degradation of organic contaminants in water with TiO₂ supported on polythene films. *J. Photochem. Photobiol. A Chem.* **1995**, *87*, 177–179. [[CrossRef](#)]
82. Castellano, M.; Cantù, R.; Mauri, M.; Marsano, E.; Vicini, S. Poly(dimethylsiloxane)/TiO₂ Photocatalytic Membranes Obtained by Different Electrospinning Systems. *J. Nanosci. Nanotechnol.* **2016**, *16*, 6587–6594. [[CrossRef](#)]
83. De Barros, A.L.; Domingos, A.A.Q.; Fechine, P.B.A.; de Keukeleire, D.; Nascimento, R.F.D. PET as a support material for TiO₂ in advanced oxidation processes. *J. Appl. Polym. Sci.* **2014**, *131*, 40175. [[CrossRef](#)]
84. Wang, F.; Min, S.X. TiO₂/polyaniline composites: An efficient photocatalyst for the degradation of methylene blue under natural light. *Chin. Chem. Lett.* **2007**, *18*, 1273–1277. [[CrossRef](#)]
85. Wahyuni, S.; Kunarti, E.S.; Swasono, R.T.; Kartini, I. Characterization and Photocatalytic Activity of TiO₂(rod)-SiO₂-Polyaniline Nanocomposite. *Indones. J. Chem.* **2018**, *18*, 321. [[CrossRef](#)]
86. Gilja, V.; Vrban, I.; Mandić, V.; Žic, M.; Hrnjak-Murgić, Z. Preparation of a PANI/ZnO Composite for Efficient Photocatalytic Degradation of Acid Blue. *Polymers* **2018**, *10*, 940. [[CrossRef](#)] [[PubMed](#)]
87. Chen, X.; Li, H.; Wu, H.; Wu, Y.; Shang, Y.; Pan, J.; Xiong, X. Fabrication of TiO₂@PANI nanobelts with the enhanced absorption and photocatalytic performance under visible light. *Mater. Lett.* **2016**, *172*, 52–55. [[CrossRef](#)]
88. Li, S.; Du, C.; Zhao, N.; Zheng, J.; Liu, H.; Wang, Y. Preparation and Application of a New-type of Ordered Macroporous PANI/TiO₂ Photocatalyst. *Chem. Lett.* **2015**, *44*, 568–570. [[CrossRef](#)]
89. Hegedűs, P.; Szabó-Bárdos, E.; Horváth, O.; Szabó, P.; Horváth, K. Investigation of a TiO₂ photocatalyst immobilized with poly(vinyl alcohol). *Catal. Today* **2017**, *284*, 179–186. [[CrossRef](#)]
90. Jiang, Y.; Chen, W.-F.; Koshy, P.; Sorrell, C.C. Enhanced photocatalytic performance of nanostructured TiO₂ thin films through combined effects of polymer conjugation and Mo-doping. *J. Mater. Sci.* **2019**, *54*, 5266–5279. [[CrossRef](#)]
91. Sekar, A.D.; Muthukumar, H.; Chandrasekaran, N.L.; Matheswaran, M. Photocatalytic degradation of naphthalene using calcined Fe ZnO/ PVA nanofibers. *Chemosphere* **2018**, *205*, 610–617. [[CrossRef](#)]
92. Montallana, A.D.S.; Vasquez, M.R., Jr. Fabrication of PVA/Ag-TiO₂ nanofiber mats for visible-light-active photocatalysis. *Results Phys.* **2021**, *25*, 104205. [[CrossRef](#)]
93. Nasikhudin; Ismaya, E.P.; Diantoro, M.; Kusumaatmaja, A.; Triyana, K. Preparation of PVA/TiO₂ Composites Nanofibers by using Electrospinning Method for Photocatalytic Degradation. In *IOP Conference Series, Proceedings of the Materials Science and Engineering, Proceedings of the 4th International Conference of Advanced Materials Science and Technology, Universitas Negeri Malang, Indonesia, 27–28 September 2016*; IOP Publishing Ltd.: Bristol, UK, 2017; Volume 202, pp. 1–7. [[CrossRef](#)]
94. Iketani, K.; Sun, R.-D.; Toki, M.; Hirota, K.; Yamaguchi, O. Sol–gel-derived TiO₂/poly(dimethylsiloxane) hybrid films and their photocatalytic activities. *J. Phys. Chem. Solids* **2003**, *64*, 507–513. [[CrossRef](#)]
95. Sosnin, I.M.; Vlassov, S.; Dorogin, L.M. Application of polydimethylsiloxane in photocatalyst composite materials: A review. *React. Funct. Polym.* **2021**, *158*, 104781. [[CrossRef](#)]
96. Lamberti, A. Microfluidic photocatalytic device exploiting PDMS/TiO₂ nanocomposite. *Appl. Surf. Sci.* **2015**, *335*, 50–54. [[CrossRef](#)]
97. Jeong, M.-G.; Seo, H.O.; Kim, K.-D.; Kim, Y.D.; Lim, D.C. Enhanced photocatalytic activity of TiO₂ by polydimethylsiloxane deposition and subsequent thermal treatment at 800 °C. *Thin Solid Films* **2012**, *520*, 4929–4933. [[CrossRef](#)]
98. Deng, Z.-Y.; Wang, W.; Mao, L.-H.; Wang, C.-F.; Chen, S. Versatile superhydrophobic and photocatalytic films generated from TiO₂-SiO₂@PDMS and their applications on fabrics. *J. Mater. Chem. A* **2014**, *2*, 4178–4184. [[CrossRef](#)]
99. Wang, T.; Lu, Z.; Wang, X.; Zhang, Z.; Zhang, Q.; Yan, B.; Wang, Y. A compound of ZnO/PDMS with photocatalytic, self-cleaning and antibacterial properties prepared via two-step method. *Appl. Surf. Sci.* **2021**, *550*, 149286. [[CrossRef](#)]
100. Santiago, A.; Gondim, J.; Tranquilin, R.; Silva, F.; Fernandez, F.; Costa, M.; Motta, F.; Bomio, M. Development of ZnO/PDMS nanocomposite with photocatalytic/hydrophobic multifunction. *Chem. Phys. Lett.* **2019**, *740*, 137051. [[CrossRef](#)]
101. Cha, B.J.; Woo, T.G.; Park, E.J.; Kim, I.H.; An, J.E.; Seo, H.O.; Kim, Y.D. Photo-catalytic activity of hydrophilic-modified TiO₂ for the decomposition of methylene blue and phenol. *Curr. Appl. Phys.* **2017**, *17*, 1557–1563. [[CrossRef](#)]
102. Barbosa, A.A.; de Aquino, R.V.S.; da Cruz Santana Neves, N.S.; Dantas, R.F.; Duarte, M.M.M.B.; da Rocha, O.R.S. Kinetic study of dye removal using TiO₂ supported on polyethylene terephthalate by advanced oxidation processes through neural networks. *Water Sci. Technol.* **2019**, *79*, 1134–1143. [[CrossRef](#)]
103. Heredia, M.; Duffy, J. Photocatalytic destruction of water pollutants using a TiO₂ film in pet bottles. In *Proceedings of the Solar Conference, Cleveland, OH, USA, 8–12 July 2007*.

104. Meichtry, J.M.; Lin, H.J.; de la Fuente, L.; Levy, I.K.; Gautier, E.A.; Blesa, M.A.; Litter, M.I. Low-Cost TiO₂ Photocatalytic Technology for Water Potabilization in Plastic Bottles For Isolated Regions. *Photocatalyst Fixation. J. Sol. Energy Eng.* **2007**, *129*, 119–126. [[CrossRef](#)]
105. Fostier, A.H.; Pereira, M.D.S.S.; Rath, S.; Guimarães, J.R. Arsenic removal from water employing heterogeneous photocatalysis with TiO₂ immobilized in PET bottles. *Chemosphere* **2008**, *72*, 319–324. [[CrossRef](#)]
106. Agustina, T.; Komala, R.; Faizal, M. Application of TiO₂ nano particles photocatalyst to degrade synthetic dye wastewater under solar irradiation. *Contemp. Eng. Sci.* **2015**, *8*, 1625–1636. [[CrossRef](#)]
107. Sanchez, L.; Guz, L.; García, P.; Ponce, S.; Goyanes, S.; Marchi, M.C.; Candal, R.; Rodriguez, J. Synthesis and Characterization of ZnO Nanorod Films on PET for Photocatalytic Disinfection of Water. *J. Adv. Oxid. Technol.* **2015**, *18*, 246–252. [[CrossRef](#)]
108. Sandoval, C.; Molina, G.; Jentsch, P.V.; Pérez, J.; Muñoz, F.; Pauker, C.F.S. Photocatalytic Degradation of Azo Dyes Over Semiconductors Supported on Polyethylene Terephthalate and Polystyrene Substrates. *J. Adv. Oxid. Technol.* **2017**, *20*, 20170006. [[CrossRef](#)]